Neutrinos from Stored Muons (νSTORM): Expression of Interest

Executive summary

Lead author: KL
Page limit: 1

To be updated!

P. Kyberd, D.R. Smith
Brunel University West London, Uxbridge, Middlesex UB8 3PH, UK
L. Coney
Department of Physics and Astronomy, University of California, Riverside, CA 92521, USA
S. Pascoli
Institute for Particle Physics Phenomenology, Department of Physics, University of Durham, Science Laboratories, South Rd, Durham, DH1 3LE, UK
D. Adey, C. Ankenbrandt, S.J. Brice, A.D. Bross, H. Cease, J. Kopp, A. Liu, N. Mokhov, J. Morfin, D. Neuffer, M. Popovic, P. Rubinov, S. Striganov
Fermilab, P.O. Box 500, Batavia, IL 60510-5011, USA
A. Blondel, A. Bravar, F. Dufour, Y. Karadhzov, A. Korzenev, E. Noah, M. Ravonel, M. Rayner, R. Asfandiyarov, A. Haesler, C. Martin, E. Scantamburlo, F. Cadoux
University de Geneve, 24, Quai Ernest-Ansermet, 1211 Geneva 4, Suisse
R. Bayes, F.J.P. Soler
School of Physics and Astronomy, Kelvin Building, University of Glasgow, Glasgow G12 8QQ, Scotland, UK
J. Kopp
Max-Planck-Institut fr Kernphysik, PO Box 103980, 69029 Heidelberg, Germany
D. Colling, A. Dobbs, J. Dobson, P. Dornan, K. Long, J. Pasternak, E. Santos, J.K. Sedgbeer, M.O. Wascko, Y. Uchida
Physics Department, Blackett Laboratory, Imperial College London, Exhibition Road, London, SW7 2AZ, UK
S.K. Agarwalla
Instituto de Fisica Corpuscular (IFIC), Centro Mixto CSIC-UVEG, Edificio Investigacion Paterna, Apartado 22085, 46071 Valencia, Spain
S.A. Bogacz
Thomas Jefferson National Laboratory, 12000 Jefferson Avenue, Newport News, VA 23606, USA
Y. Mori, J.B. Lagrange
Kyoto University, Research Reactor Institute, 2,Asashiro-Nishi, Kumatori-cho, Sennan-gun, Osaka 590-0494 Japan
A. de Gouvêa
Northwestern University, Dept. of Physics and Astronomy, 2145 Sheridan Road, Evanston, Illinois 60208-3112 USA
Y. Kuno, A. Sato
Osaka University, Graduate School, School of Science, 1-1 Machikaneyama-cho, Toyonaka, Osaka 560-0043, Japan
V. Blackmore, J. Cobb, C. D. Tunnell, A. Webber
Particle Physics Department, The Denys Wilkinson Building, Keble Road, Oxford, OX1 3RH, UK
K.T. McDonald
Princeton University, Princeton, NJ, 08544, USA
G. Hanson
Department of Physics and Astronomy, University of California, Riverside, CA 92521, US
R. Edgecock, S. Ricciardi, C. Rogers
STFC Rutherford Appleton Laboratory, Chilton, Didcot, Oxfordshire, OX11 0QX, UK
C. Booth
University of Sheffield, Dept. of Physics and Astronomy, Hicks Bldg., Sheffield S3 7RH, UK

M. Dracos, N. Vassilopoulos
IPHC, Université de Strasbourg, CNRS/IN2P3, F-67037 Strasbourg, France
J.M. Link, P. Huber
Virginia Polytechnic Inst. and State Univ., Physics Dept., Blacksburg, VA 24061-0435
J.J. Back, S.B. Boyd, P.F. Harrison
Department of Physics, University of Warwick, Coventry, CV4 7AL, UK
J.T. Sobczyk
Institute of Theoretical Physics, University of Wroclaw, pl. M. Borna 9,50-204, Wroclaw, Poland
W. Winter
Fakultät für Physik und Astronomie, Am Hubland, 97074 Würzburg, Germany

Contents

1 Introduction

1.1 Overview

Neutrino oscillations are readily described in terms of three neutrino-mass eigenstates and a unitary mixing matrix that relates the mass states to the flavour states (the Standard Neutrino Model, SνM) [1, 2, 3, 4]. The three-neutrino-mixing paradigm is able to give an accurate description of measurements of neutrinos and anti-neutrinos produced in the sun, by cosmic ray interactions in the atmosphere, by high-energy particle accelerators and anti-neutrinos produced by nuclear reactors [5]. However, a number of results can not be described by the SνM. First, the LSND collaboration reported evidence for $\bar{\nu}_\mu \rightarrow \bar{\nu}_e$ oscillations corresponding to a mass-squared difference of $\sim 1\,\mathrm{eV}^2$ [6]; a value which is much larger than the two mass-squared differences of the SνM. A third mass-squared difference, if confirmed, would imply a fourth neutrino-mass state and hence the existence of a sterile neutrino. The MiniBooNE experiment observed an effect consistent with the LSND result [7, 8]. A further hint for the existence of sterile neutrinos may be provided by the discrepancy between the measured reactor-neutrino flux and that obtained in new calculations of the expected flux [9, 10, 11]. Finally, the GALLEX and SAGE experiments reported anomalies in the rate of neutrinos observed from the sources used to calibrate their radio-chemical detection techniques [12, 13, 14, 15, 16]. A detailed review of the relevant data may be found in [17].

Unambiguous evidence for the existence of one or more sterile neutrinos would revolutionise the field. The νSTORM experiment described in this Expression of Interest (EoI) is capable of making the measurements required to confirm or refute the evidence for sterile neutrinos summarised above using a technique that is both qualitatively and quantitatively new [18]. The νSTORM facility has been designed to deliver beams of ν_e ($\bar{\nu}_e$) and $\bar{\nu}_\mu$ (ν_μ) from the decay of a stored muon beam with a central momentum of 3.8 GeV and a momentum spread of 10% [18]. A detector located at a distance $\sim 2\,000$ m from the end of one of the straight sections will be able to make sensitive searches for the existence of sterile neutrinos. If no appearance ($\bar{\nu}_\mu \rightarrow \bar{\nu}_e$) signal is observed, the LSND allowed region can be ruled out at the $\sim 10\sigma$ level. Instrumenting the νSTORM neutrino beam with a near detector at a distance of ~ 50 m makes it possible to search for sterile neutrinos in the disappearance $\nu_e \rightarrow \nu_X$ and $\nu_\mu \rightarrow \nu_X$ channels. In the disappearance search, the absence of a signal would allow the presently allowed region to be excluded at the 90% confidence level.

Now that the small mixing angle θ_{13} is known [19, 20, 21, 22, 23], the emphasis of the study of the SνM has shifted to the determination of the mass hierarchy and the search for CP-invariance violation. In a conventional super-beam experiment, both of these objectives requires the measurement of ν_e ($\bar{\nu}_e$) appearance in a ν_μ ($\bar{\nu}_\mu$) beam. With a sufficiently large data sample, the measurement of the mass hierarchy is relatively insensitive to systematic uncertainties. By contrast, the sensitivity to CP-invariance violation depends critically on systematic effects in general and on the knowledge of the $\nu_e N$ ($\bar{\nu}_e N$) cross sections in particular [24, 25]. The νSTORM facility described in this EoI is unique in that it is capable of serving a near detector (or suite of near detectors) that will be able to measure $\nu_e N$ ($\bar{\nu}_e N$) and $\nu_\mu N$ ($\bar{\nu}_\mu N$) cross sections at the percent level and of studying the hadronic final states in detail.

By providing the ideal technology test-bed, the νSTORM facility will play a pivotal role in the development of neutrino detectors, accelerator systems and instrumentation techniques. It is capable of supporting the development of the high-resolution, totally-active, magnetised neutrino detectors that are required for the incremental development of the long- and short-baseline neutrino-oscillation programmes. The development of the νSTORM ring, together with the instrumentation required for the νN-scattering and sterile-neutrino-search programmes will allow the next step in the development of muon accelerators for particle physics to be defined. Just as the Cambridge Electron Accelerator [26], built by Harvard and MIT at the end of the '50s, was the first in a series of electron synchrotrons that culminated in LEP, νSTORM has the potential to establish a new tech-

nique for particle physics that can be developed to deliver the high-energy ν_e ($\bar{\nu}_e$) beams required to elucidate the physics of flavour at the Neutrino Factory [27] and to provide the basis for multi-TeV lepton-antilepton collisions at the Muon Collider [28].

1.2 νSTORM and the emerging CERN neutrino programme

1.2.1 Short-baseline neutrino facility in the North Area

It has been proposed to develop the North Area at CERN to host a portfolio of neutrino experiments. In the short term, it has been proposed that a search for sterile neutrinos be carried out by the ICARUS and NESSiE collaborations. These experiments will be served by a conventional neutrino beam generated by the fast extraction of protons from the SPS at 100 GeV. For these experiments to take sufficient data before the second long shutdown of the LHC in 2017 requires that the beam and experiments be implemented such that data taking can start early in 2016. νSTORM requires a primary proton beam similar to that which is being prepared for ICARUS/NESSiE but with a smaller transverse and longitudinal emittance. A beam with the appropriate properties will be available once LINAC4 becomes operational after the 2017 long shutdown. The near and far source–detector distances required by νSTORM closely match those specified for ICARUS/NESSiE.

The concept for the implementation of the νSTORM facility at CERN presented in this EoI is self-consistent and is capable of delivering searches for sterile neutrinos with exquisite sensitivity and serving a unique and detailed $\nu_e N$ ($\bar{\nu}_e N$) scattering programme. Given the technical synergies, it is natural to consider how the νSTORM facility could be developed first to enhance and then to take forward the short-baseline neutrino programme at CERN.

1.2.2 Long-baseline neutrino oscillation physics

The present generation of long-baseline neutrino-oscillation experiments (MINOS, T2K, NOνA) will continue to refine the measurements of the mixing parameters. Their data, taken together with that obtained in atmospheric-neutrino experiments, may constrain the neutrino mass hierarchy at the 2σ—3σ confidence level. However, even in combination with all oscillation data, the present generation of experiments will be essentially insensitive to leptonic CP-invariance violation.

High-power conventional neutrino beams serving very large detectors have been proposed to determine the mass hierarchy. Such "super-beam" experiments fall into two broad categories: narrow-band beams, in which a low-energy ($E_\nu \leq 1$ GeV) beam is used to illuminate a detector 100 km—300 km from the source; and wide-band beams in which neutrinos with energies spanning the range ~ 1 GeV to 10 GeV illuminate a detector at a distance of between 700 km and 2 300 km from the source.

The opportunities for CERN to host a next-generation super-beam has been studied by the EUROν Framework Programme 7 (FP7) Design Study consortium. EUROν studied a narrow-band beam generated using the 5 GeV, 4 MW Superconducting Proton Linac (SPL) at CERN illuminating the MEMPHYS, 450 kT water Cherenkov detector located in the Laboratoire Souterrain de Modane (LSM) at a distance of 130 km (this option is referred to as CERN-Frejus since the LSM is located in the Frejus tunnel).

The study of super-beam experiments at CERN is now being taken forward by the LAGUNA-LBNO FP7 Design Study consortium. In LAGUNA-LBNO, the CERN-Frejus narrow-band beam continues to be developed and a new wide-band beam option, the Long-Baseline Neutrino Observatory (LBNO), is being considered. LBNO calls for a high-energy, wide-band neutrino beam to be created using protons from the SPS. The beam would serve a suite of detectors in the Pyhäsalmi mine in Finland, at a distance of 2 300 km from CERN. The

long baseline, coupled with the wide-band makes the CERN-Pyhäsalmi option unique in that it would allow LBNO to determine the mass hierarchy at a confidence level in excess of 5σ no matter what the value of the CP phase. Alternative proposals for next generation super-beam experiments have been brought forward in Japan (the Tokai to Hyper-Kamiokande, T2HK, experiment) and in the US (the Long-Baseline Neutrino Experiment, LBNE).

Each of the super-beam experiments outline above exploits the sub-leading $\nu_\mu \to \nu_e$ ($\bar{\nu}_\mu \to \bar{\nu}_e$) oscillation to determine the mass hierarchy and to search for leptonic CP-invariance violation. At present, data on neutrino-nucleus scattering in the energy range of interest is limited to relatively sparse $\nu_\mu N$ ($\bar{\nu}_\mu N$) measurements; $\nu_e N$ ($\bar{\nu}_e N$) cross sections being inferred from the $\nu_\mu N$ ($\bar{\nu}_\mu N$) measurements. As a result, uncertainties in oscillation measurements made using conventional beams suffer from systematic uncertainties arising from the absence of reliable electron-neutrino-nucleus (and muon-neutrino-nucleus) scattering cross sections. Moreover, the lack of knowledge of the relevant cross sections gives rise to correlated uncertainties in the estimate of the neutrino-beam flux.

νSTORM has the potential to make detailed studies of both $\nu_e N$ ($\bar{\nu}_e N$) and $\nu_\mu N$ ($\bar{\nu}_\mu N$) scattering. As discussed in this EoI, an appropriately designed suite of near detectors will be able to determine the scattering cross sections and provide detailed information on the hadronic final states. The latter will be of first importance not only in the long-baseline oscillation programme, but will allow the systematic study of the sources of background that currently affect sterile neutrino searches. The cross-section measurements that νSTORM will provide will therefore be an essential part of the emerging CERN neutrino programme.

1.2.3 A step on the way to the Neutrino Factory

To go beyond the sensitivity offered by the next generation super-beam experiments requires the development of novel techniques for the production of neutrino beams and novel detector systems. Pure ν_e ($\bar{\nu}_e$) beams may be generated from the decay of radioactive ions at a "beta-beam" facility. The low charge-to-mass ratio of the ions places a practical limit of ~ 1 GeV on the neutrino energies that can be produced in this way. Alternatively, high-energy electron- and muon-neutrino beams of precisely known flux may be generated from the decay of stored muon beams at the Neutrino Factory.

The Neutrino Factory has been shown to offer a sensitivity to CP-invariance violation superior to that which can be achieved at any other proposed facility. The EUROν consortium demonstrated that the CERN baseline ($\gamma = 100$) beta-beam becomes competitive only if it is combined with the CERN-Frejus super-beam, or a super-beam of comparable performance. Detailed and precise measurements of neutrino oscillations will be required for the physics of flavour to be elucidated. The challenge to the experimental community is to establish a programme capable of delivering measurements of the neutrino-mixing parameters with a precision approaching that with which the quark mixing parameters are known. Only the Neutrino Factory offers such precision.

It is conceivable that the Neutrino Factory can be implemented in a series of increments or stages—each increment offering a first-rate neutrino-science programme and being capable of delivering the R&D required for the development of the subsequent increment. The International Design Study for the Neutrino Factory (IDS-NF) collaboration will include a discussion of the incremental implementation of the facility in its Reference Design Report that will be published in the autumn of 2013. The νSTORM facility, by proving the feasibility of using stored muon beams to provide neutrino beams for physics, will be the essential first increment.

2 Motivation

2.1 Sterile neutrino search

2.1.1 Sterile neutrinos in extensions of the Standard Model

Sterile neutrinos—fermions that are uncharged under the $SU(3) \times SU(2) \times U(1)$ gauge group—arise naturally in many extensions of the Standard Model and even where they are not an integral part of a model, they can usually be accommodated easily. A detailed overview of sterile neutrino phenomenology and related model building considerations is given in [17].

For instance, in Grand Unified Theories (GUTs), fermions are grouped into multiplets of a large gauge group, of which $SU(3) \times SU(2) \times U(1)$ is a subgroup. If these multiplets contain not only the known quarks and leptons, but also additional fermions, these new fermions will, after the breaking of the GUT symmetry, often behave like gauge singlets (see for instance [29, 30, 31, 32] for GUT models with sterile neutrinos).

Models attempting to explain the smallness of neutrino masses through a see-saw mechanism generically contain sterile neutrinos. While in the most generic see-saw scenarios, these sterile neutrinos are extremely heavy ($\sim 10^{14}$ GeV) and have very small mixing angles ($\sim 10^{-12}$) with the active neutrinos, slightly non-minimal see-saw models can easily feature sterile neutrinos with eV-scale masses and with per cent level mixing with the active neutrinos. Examples for non-minimal see-saw models with relatively light sterile neutrinos include the split see-saw scenario [33], see-saw models with additional flavour symmetries (see e.g. [34]), models with a Froggatt-Nielsen mechanism [35, 36], and extended see-saw models that augment the mechanism by introducing more than three singlet fermions, as well as additional symmetries [37, 38, 39].

Finally, sterile neutrinos arise naturally in "mirror models", in which the existence of an extended "dark sector", with nontrivial dynamics of its own, is postulated. If the dark sector is similar to the visible sector—as is the case, for instance in string-inspired $E_8 \times E_8$ models—it is natural to assume that it also contains neutrinos [40, 41, 42].

2.1.2 Experimental hints for light sterile neutrinos

While the theoretical motivation for the existence of sterile neutrinos is certainly strong, what has mostly prompted the interest of the scientific community in this topic is the fact that there are several experimental results that show deviations from the Standard Model predictions which can be interpreted as hints for oscillations involving light sterile neutrinos with masses of order eV.

The first of these hints was obtained by the LSND collaboration, who carried out a search for $\bar{\nu}_\mu \to \bar{\nu}_e$ oscillations over a baseline of $\sim$ 30 m [6]. Neutrinos were produced in a stopped pion source in the decay $\pi^+ \to \mu^+ + \nu_\mu$ of pions at rest and the subsequent decay $\mu^+ \to e^+ \bar{\nu}_\mu \nu_e$. Electron anti-neutrinos were detected through the inverse beta decay reaction $\bar{\nu}_e p \to e^+ n$ in a liquid scintillator detector. Backgrounds to this search arise from the decay chain $\pi^- \to \bar{\nu}_\mu + (\mu^- \to \nu_\mu \bar{\nu}_e e^-)$ if negative pions produced in the target decay before they are captured by a nucleus, and from the reaction $\bar{\nu}_\mu p \to \mu^+ n$, which is only allowed for the small fraction of muon anti-neutrinos produced by pion decay *in flight* rather than stopped pion decay. The LSND collaboration found an excess of $\bar{\nu}_e$ candidate events above this background with a significance of more than 3σ. When interpreted as $\bar{\nu}_\mu \to \bar{\nu}_e$ oscillations through an intermediate sterile state $\bar{\nu}_s$, this result is best explained by sterile neutrinos with an effective mass-squared splitting $\Delta m^2 \gtrsim 0.1$ eV^2 relative to the active neutrinos, and with an effective sterile sector-induced $\bar{\nu}_\mu$–$\bar{\nu}_e$ mixing angle $\sin^2 2\theta_{e\mu,\text{eff}} \gtrsim 2 \times 10^{-3}$, depending on Δm^2.

The MiniBooNE experiment [43] was designed to test the neutrino oscillation interpretation of the LSND

result using a different technique, namely neutrinos from a horn-focused pion beam. By focusing either positive or negative pions, MiniBooNE could run either with a beam consisting mostly of neutrinos or in a beam consisting mostly of anti-neutrinos. In both modes, the experiments observed an excess of electron-like events at sub-GeV energies. The excess has a significance above 3σ and can be interpreted in terms of $\overset{(-)}{\nu}_\mu \to \overset{(-)}{\nu}_e$ oscillations consistent with the LSND observation [43].

A third hint for the possible existence of sterile neutrinos is provided by the reactor anti-neutrino anomaly. In 2011, Mueller et al. published a new ab initio computation of the expected neutrino fluxes from nuclear reactors [9]. Their results improve upon a 1985 calculation by Schreckenbach [44] by using up-to-date nuclear databases, a careful treatment of systematic uncertainties and various other corrections and improvements that were neglected in the earlier calculation. Mueller et al. find that the predicted anti-neutrino flux from a nuclear reactor is about 3% higher than previously thought. This result, which was later confirmed by Huber [10], implies that short baseline reactor experiments have observed a *deficit* of anti-neutrinos compared to the prediction [11, 17]. It needs to be emphasised that the significance of the deficit depends crucially on the systematic uncertainties associated with the theoretical prediction, some of which are difficult to estimate reliably. If the reactor anti-neutrino deficit is interpreted as $\bar{\nu}_e \to \bar{\nu}_s$ disappearance via oscillation, the required 2-flavour oscillation parameters are $\Delta m^2 \gtrsim 1$ eV^2 and $\sin^2 2\theta_{ee,\text{eff}} \sim 0.1$.

Short-baseline oscillations in this parameter range could also explain another experimental result: The Gallium anomaly. The GALLEX and SAGE solar neutrino experiments used electron neutrinos from intense artificial radioactive sources to demonstrate the feasibility of their radio-chemical detection principle [12, 13, 14, 15, 16]. Both experiments observed fewer ν_e from the source than expected. The statistical significance of the deficit is above the 99% confidence level and can be interpreted in terms of short-baseline $\bar{\nu}_e \to \bar{\nu}_s$ disappearance with $\Delta m^2 \gtrsim 1$ eV^2 and $\sin^2 2\theta_{ee,\text{eff}} \sim 0.1$–$0.8$. [45, 46, 47].

2.1.3 Constraints and global fit

While the previous section shows that there is an intriguing accumulation of hints for the existence of new oscillation effects—possibly related to sterile neutrinos—in short-baseline experiments, these hints are not undisputed. Several short-baseline oscillation experiments (KARMEN [48], NOMAD [49], E776 [50], ICARUS [51], atmospheric neutrinos [52], solar neutrinos [53, 54, 55, 56, 57, 58, 59, 60, 61, 62], MINOS [63, 64], and CDHS [65]) did *not* confirm the observations from LSND, MiniBooNE, reactor experiments, and Gallium experiments, and place very strong limits on the relevant regions of parameter space in sterile neutrino models. To assess the viability of these models it is necessary to carry out a global fit to all relevant experimental data sets, and several groups have endeavoured to do so [66, 67, 68, 69, 70, 17]. In figure 1, which is based on the analysis presented in [66, 17, 71], we show the current constraints on the parameter space of a $3 + 1$ model (a model with three active neutrinos and one sterile neutrino). We have projected the parameter space onto a plane spanned by the mass-squared difference Δm^2 between the heavy, mostly sterile mass eigenstate and the light, mostly active ones and by the effective amplitude $\sin^2 2\theta_{e\mu,\text{eff}}$ for sterile-mediated $\nu_\mu \to \nu_e$ oscillations.

We see that there is severe tension in the global data set: The parameter region flavoured by the hints from LSND, MiniBooNE, reactor neutrinos and gallium experiments is incompatible, at the 99% confidence level, with constraints from other experiments. Similarly, the parameter region flavoured by the global $\overset{(-)}{\nu}_e$ appearance data, has only very little overlap with the region flavoured by $\overset{(-)}{\nu}_\mu$ and $\overset{(-)}{\nu}_e$ disappearance experiments. Using a parameter goodness of fit test [92] to quantity this tension, p-values on the order of few $\times\, 10^{-5}$ are found for the compatibility of appearance and disappearance data. The global fit improves somewhat in models with more than one sterile neutrino, but significant tension remains [66, 17].

One can imagine several possible resolutions to this puzzle:

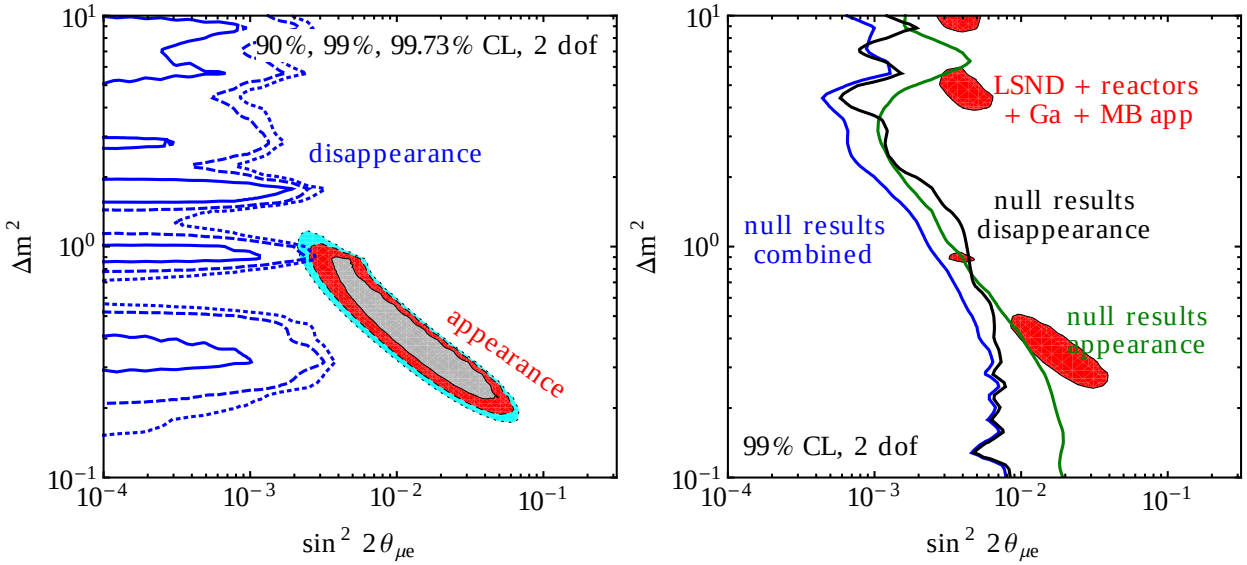

Figure 1: Global constraints on sterile neutrinos in a 3+1 model. In the left panel, we show that $\overset{(-)}{\nu}_e$ appearance data (coloured region: LSND [6], MiniBooNE [43], KARMEN [48], NOMAD [49], E776 [50], ICARUS [51]) is only marginally consistent with disappearance data (blue contours: atmospheric neutrinos [52], solar neutrinos [53, 54, 55, 56, 57, 58, 59, 60, 61, 62], MiniBooNE/SciBooNE [72, 73] MINOS [63, 64], reactor experiments [74, 75, 76, 77, 78, 79, 80, 81, 82, 83, 20, 84], CDHS [65], KARMEN [85] and LSND [86] ν_e–^{12}C scattering data and gallium experiments [13, 15, 54, 16]). In the right panel, we have split the data into those experiments which see unexplained signals (LSND, MiniBooNE appearance measurements, reactor experiments, gallium experiments) and those which don't. For the analysis of reactor data, we have used the new reactor flux predictions from [9], but we have checked that the results, especially regarding consistency with LSND and MiniBooNE $\bar{\nu}$ data, are qualitatively unchanged when the old reactor fluxes are used. Fits have been carried out in the GLoBES framework [87, 88] using external modules discussed in [89, 90, 91, 71].

1. One or several of the apparent deviations from the SνM oscillation framework discussed in section 2.1.2 have explanations not related to sterile neutrinos;
2. One or several of the null results that favour the no-oscillation hypothesis is or are in error;
3. There are more than two sterile neutrino flavours. Note that already scenarios with one sterile neutrino with an eV scale mass are in some tension with cosmology (see, however, [93]), but the existence of one sterile neutrino with a mass well below 1 eV is actually preferred by cosmological fits [94, 95, 96, 97]. Cosmological bounds on sterile neutrinos can be avoided in non-standard cosmologies [98] or by invoking mechanisms that suppress sterile neutrino production in the early universe [99, 100]; and
4. There are sterile neutrinos plus some other kind of new physics at the eV scale (see for instance [91, 101] for an attempt in this direction).

We conclude that our understanding of short baseline neutrino oscillations is currently in a rather unsatisfactory state. On the one hand, several experiments hint at deviations from the established three-neutrino framework. However, none of these hints can be considered conclusive, and moreover, when interpreted in the simplest sterile neutrino models, they are in severe tension with existing constraints on the parameter space of these models. An experiment searching for short-baseline neutrino oscillations with good sensitivity and well-controlled systematic uncertainties has great potential to clarify the situation by either finding a new type of neutrino oscillation or by deriving a strong and robust constraint on any such oscillation. While the former outcome would constitute a major discovery, the latter would also receive a lot of attention since it would provide the world's strongest constraints on a large variety of theoretical models postulating "new physics" in the neutrino sector at the eV scale.

2.2 Neutrino-nucleus scattering

2.2.1 Introduction

To date, neutrino oscillations [102] remain the only observed and confirmed phenomenon not allowed by the Standard Model (SM) of particle physics. Neutrino oscillation data, combined with searches for kinematic effects of neutrino mass in tritium decay experiments, very clearly indicate that, in a 3-ν paradigm, the mass of the heaviest neutrino must be smaller than ~ 1 eV. This mass is too small to be naturally explained by the Higgs mechanism, which is why the discovery of neutrino mass and mixing is clearly beyond the SM. The detailed exploration of the neutrino sector is one of the most important goals for the next decade in particle physics research, and the neutrino community is converging on the conclusion that a wide-band long-baseline (LBL) accelerator neutrino experiment is the best next step in that research programme [103, 104, 105], with the main goals of discovering the neutrino mass hierarchy and searching for CP-invariance violation in the lepton sector. Recent observations that the value of the third neutrino mixing angle, θ_{13}, is relatively large [22, 19, 20] mean that the rates of ν_e or $\bar{\nu}_e$ appearance in a wide-band beam will be substantial, and that the measurements will be dominated by systematic uncertainties, especially errors on the modelling of neutrino-nucleus scattering. Thus, it is crucial to reduce these systematic uncertainties in order to achieve the stated goals for the precision of the next generation wide-band beam, long-baseline oscillation programme.

The current generation of neutrino oscillation experiments employ neutrino-interaction models developed in the 1970's and 80's [106, 107, 108]. In the energy region of interest to the LBL programme ($0.1 - 10$ GeV) the dominant reaction types, in order of threshold, are quasi-elastic scattering, resonant and coherent pion production, and deep inelastic scattering. High statistics neutrino scattering measurements made in the past decade by K2K [109, 110, 111, 112], MiniBooNE [113, 114, 115, 116, 117, 118, 119], and SciBooNE [120, 121, 122, 123] indicate that the quasi-elastic scattering and pion production models do not describe Nature; details of these physics issues are discussed below in sections 2.2.2 and 2.2.3.

Even with this degree of activity, the precision with which the basic neutrino-*nucleon* cross sections are known is still not better than $20-30\%$. There are two main reasons for this: the poor knowledge of neutrino fluxes and the fact that all the recent cross section measurements have been performed on nuclear targets. It is important to recall that current neutrino experiments measure events that are a convolution of energy-dependent neutrino flux $\otimes$ energy-dependent cross section $\otimes$ energy-dependent nuclear effects. Experiments have, for example, measured an effective neutrino-carbon cross section, and extracting a neutrino-nucleon cross section from these measurements requires separating nuclear-physics effects that can be done with only limited precision. For many oscillation experiments, using the same nuclear targets for their near and far detectors is a good start. However, even with the same nuclear target near-and-far, the presence of oscillations leads to different neutrino fluxes at the near and far detectors. That means there is a different convolution of cross section $\otimes$ nuclear effects near and far, so there is no automatic cancellation between the near-and-far detectors at the precision level needed for the LBL programme. Furthermore, these effects are exacerbated in measurements of anti-neutrino cross sections because the event rates are significantly reduced. And finally, the intrinsic differences between ν_μ and ν_e interaction cross sections must be measured with a precision commensurate with the precision goals of the LBL programme; section 2.2.4 discusses these differences in detail.

In summary, to ensure a successful LBL programme, a thorough comparison of measured neutrino-nucleon cross sections with theoretical models is needed so that all these convoluted effects can be understood.

2.2.2 Charged-current quasi-elastic scattering

Neutrino-nucleon charged-current quasi-elastic (CCQE) scattering, $\nu_l\ n \rightarrow l^-\ p$, is the most abundant neutrino reaction in the 1 GeV energy region and also the most important one in investigations of the oscillation signal. Despite its importance and apparent simplicity, the CCQE cross section is known with limited accuracy. The main reasons for the poor understanding of this reaction[124, 125] are the large neutrino flux uncertainties (both in overall normalisation and energy shape), and the fact that all recent CCQE cross-section measurements were made on bound nucleons with many complications coming from nuclear effects.

In the standard theoretical approach to describe the CCQE cross section, a weak-current transition matrix element is expressed in terms of three independent form-factors. The two vector form-factors are known from electron scattering experiments, thanks to the conserved vector-current hypothesis. Assuming the partially conserved axial-current hypothesis leaves one independent axial-vector form-factor for which one usually assumes a dipole form, and this, in turn, leaves only one free parameter: the axial mass (M_A). Within this simple theoretical framework, an investigation of CCQE scattering is equivalent to an M_A measurement. Experience from electron scattering tells us that dipole expressions provide a reasonable approximation to electric and magnetic form factors, and *extrapolation* of this argument to the axial form factors seems to be a justified, though not completely obvious, assumption. M_A determines both the overall CCQE cross section and also the shape of the distribution of events in Q^2, the square of four-momentum transfer. The preferred way to measure M_A is to analyse the shape of the $d\sigma/dQ^2$ spectrum because this mitigates the dependence on the overall flux normalisation.

Another problem with measuring the CCQE cross section stems from the fact that all neutrino fluxes are wide band beams and so it is difficult to separate the various dynamical mechanisms in neutrino-nucleon (-nucleus) interactions. The situation is much more complex than for electron scattering where good knowledge of the initial and final electron states allows a model-independent measurement of Q^2. For these reasons, neutrino cross-section measurements are always inclusive and there is even reason to consider the limitations of the commonly assumed impulse approximation [126], which stipulates that the neutrino interacts with an individual bound nucleon and that one can thus neglect collective effects. (All the major MC event generators do not include (continuous) random phase approximation corrections).

Nuclear effects include, first of all, Fermi motion and nucleon binding effects. Clearly, in investigations of CCQE, it is important to use the best Fermi motion models, which means employing the spectral function formalism [127] that has been validated in electron scattering. Moreover, in the last three years it has become clear that we must also consider a two body current contribution to the cross section [128, 129]; these currents give rise to events that can be easily confused with genuine CCQE events unless one carefully investigates final-state nucleons.

Recent interest in CCQE scattering was triggered by several large M_A measurements, and in particular by the high-statistics muon double-differential cross section on carbon from the MiniBooNE experiment [114]. Here, *large* is relative to values obtained from older, mostly light nuclear target, neutrino [130] and pion electroproduction data [131]. The MiniBooNE detector is not sensitive to final-state nucleons, which are produced below Cherenkov threshold. What MiniBooNE measures can be described as *CCQE-like* events—defined as those with no pion in the final state—with data-driven corrections for the contribution from pion production and absorption. Several theoretical groups have attempted to explain the MiniBooNE CCQE double-differential cross-section data with models containing significant contributions from np-nh mechanisms, which allow n particles and n holes, with $n \geq 2$, in the final state (np-nh mechanisms are also called meson exchange currents (MEC), multi-nucleon knock-out, or two-body currents). The Valencia/IFIC group performed a fit with its model to the two-dimensional MiniBooNE CCQE data, obtaining $M_A = 1.077 \pm 0.027$ GeV [132]. Good qualitative agreement was obtained by the Lyon [133] group. These two models are shown compared to (one muon angular bin of) MiniBooNE double-differential muon data in figure 2. Qualitative agreement has also been obtained with an optical potential model [134], while slightly worse agreement was found with the super-scaling approach [135] and transverse enhancement (TE) model [136, 137]. A general observation is that theoretical models are usually able to explain the normalisation effect of the large M_A value from MiniBooNE but their predictions do not agree with the full two-dimensional muon data set.

Theoretical models of the MEC contribution give quite different estimates of the significance of the effect in the case of anti-neutrino scattering. Recently, MiniBooNE showed the first high-statistics anti-neutrino CCQE cross section and in particular a ratio of neutrino and anti-neutrino *CCQE-like* cross sections (defined as explained above) as a function of energy. These data may allow some comparison between the models, but higher precision data on multiple nuclear targets is needed.

For CCQE events one can calculate the energy of the incoming neutrino using just the final charged lepton three-momentum, assuming the target nucleon was at rest. Clearly, the effects of Fermi motion and binding energy limit the accuracy of the neutrino energy reconstruction and introduce some model-dependent bias. The neutrino energy is used for oscillation studies since that is the only experimental parameter which affects the oscillation probability. Additional complications come from events which mimic CCQE interactions, e.g., from real pion production and absorption. The MiniBooNE data for the muon double differential cross section can be described using the standard CCQE model with a large value of M_A (although it is better to call this an effective parameter M_A^{eff} as proposed in [113]). However, use of the CCQE model with M_A^{eff} in the oscillation signal analysis surely introduces some bias since the presence of two-body current contributions changes the mapping from neutrino energy to charged lepton momentum, as noted by several recent studies [**?**, 125, 138, 139, 140].

Separation of two-body current contributions should be possible by looking at final-state nucleons [139, 141]. This is however a very challenging goal to achieve because of nucleon final-state interactions and also contamination from real pion production and absorption events. One needs very good resolution of final-state nucleons with a low threshold for the momentum of reconstructed tracks. Liquid argon TPCs have been suggested as candidate instruments to improve MC cascade models [**?**].

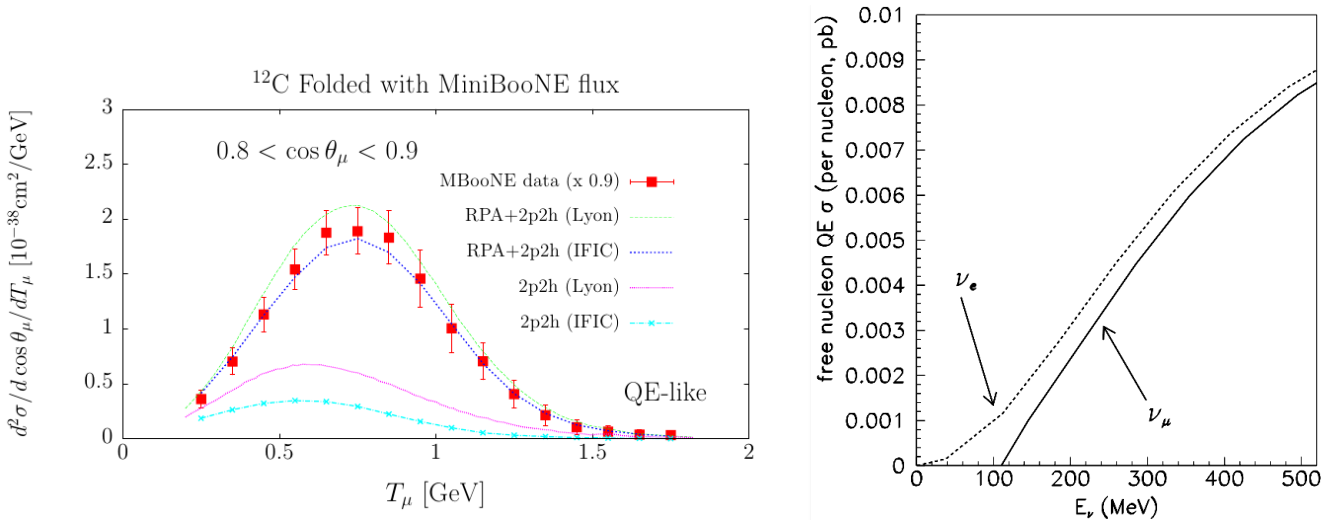

Figure 2: (left) MiniBooNE flux averaged CCQE-like cross section normalised per neutron with experimental points rescaled by 0.9. $\cos\theta_\mu \in (0.8, 0.9)$. Predictions from two theoretical models are compared and contributions from np-nh mechanism are also shown separately. (right) The total charged-current quasi-elastic cross-section for ν_μ and ν_e neutrinos.

2.2.3 Resonance Region

The neutrino interaction landscape in the few-GeV region is a complex mix of resonance production, shallow inelastic scattering physics where resonance production merges into deep inelastic scattering, and coherent processes. The dominant production mechanism in this region is the production of a $\Delta(1232)$ baryon, followed by its decay to a single pion final state. A challenging process to study experimentally, most experiments are complicated by the fact that the neutrinos interact in an extended nuclear target: the final state particles must leave the nucleus to be observed and along the way can be scattered, absorbed or undergo charge-exchange reactions. These final-state interactions must somehow be decoupled from the underlying neutrino-nucleon cross-sections—a process which is model-dependent—making interpretation of the data challenging. The resonance production channel presents the largest background to current neutrino oscillation experiments and it is therefore important to understand its contribution. Moreover, future experiments such as LBNE [103] and LBNO [104, **?**] are designed to operate at neutrino energies of 3-7 GeV where this transition region between quasi-elastic scattering and deep inelastic scattering is most important. For these experiments, a much better understanding of this region is required if they are to have maximum sensitivity to CP-invariance violation in the neutrino sector.

The quality of experimental data in the resonance region is varied. Whilst there has been recent work on neutrino-induced single-pion production mechanisms in experiments such as MiniBooNE, data on multi-pion and other final-state production mechanisms are sparse or non-existent. Figure **??** (left) shows, for example, the only current data on the $\nu_\mu p \to \nu_\mu n\pi^+$ channel. The state of knowledge of this channel is not uncommon. In recent years experiments such as K2K [145, 110, 146], MiniBooNE [116, 114, 115] and SciBooNE [122, 123] have presented data on neutral-current π^0 (NC π^0) production, charged current π^+ (CC π^+) production and the charged current π^0 (CC π^0) channel. Improved knowledge of the NC π^0 production cross section is vital as it is a dominant systematic error in ν_e appearance oscillation experiments. The CC π^+ and CC π^0 channels have been studied by MiniBooNE[116] which has produced differential cross sections in the final-state particle momenta and angles. The cross section results differ from the current Monte Carlo models by up to 20% in the case of the charged-pion mode and by up to a factor of two for the neutral-pion mode, suggesting a discrepancy

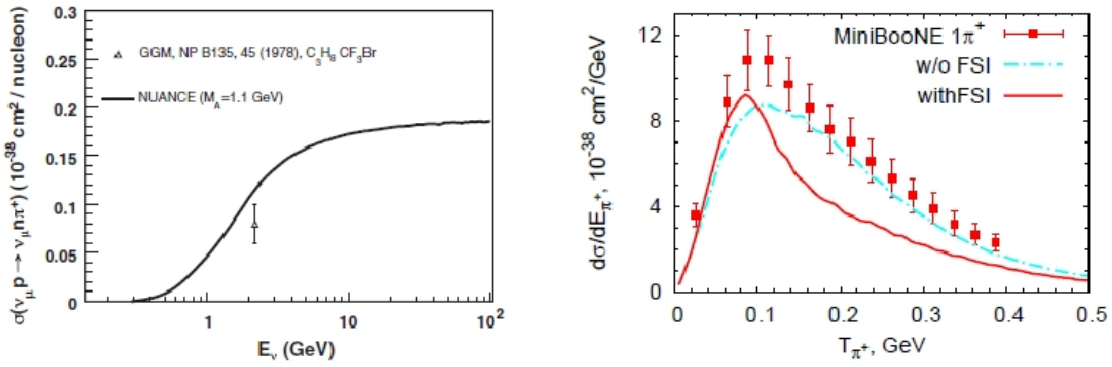

Figure 3: (left) Existing measurements of the $\nu_\mu p \rightarrow \nu_\mu n \pi^+$ cross section as a function of neutrino energy[142]. Data points come from the Gargamelle bubble chamber data[143]. The line is the prediction from the NUANCE Monte Carlo event generator. (right) Distribution of $\nu_\mu C \rightarrow \mu^- \pi^+ X$ cross section as a function of the pion momentum from the GIBBU simulation [144], compared with MiniBooNE data[117].

in both the understanding of the neutrino-nucleon cross section and the final state effects. Figure 3 (right) shows the differential cross section for CC π^+ production on ^{12}C as a function of pion kinetic energy from MiniBooNE compared to the sophisticated GiBUU simulation[144]. The model appears to favour no, or at least a very small, component of final-state interactions even though it is known that final-state interactions have a large effect. The solution to this puzzle lies in understanding both the neutrino-nucleon cross section and final-state effects independently. Such a program of study would involve the comparison of the final-state topologies of the CC π reaction on different nuclei. A critical element, however, is knowledge of the neutrino-nucleon cross section on an H_2 or D_2 target. This is an anchor point, allowing the analysers to tune their models to the bare cross section before comparison with nuclear data. Light nucleon data was last taken by the bubble-chamber experiments in the 1970's and 1980's. More complete, and better understood, data on light nuclei is now necessary to understand the resonance production models. A dedicated light target detector in the νSTORM facility is therefore of interest. It should be emphasised that this is the state of data from neutrino-induced interactions. Data on anti-neutrino resonance production are even more sparse and there does not exist any data on resonance production in an electron-neutrino beam. One of the primary means of studying CP-invariance violation is to investigate differences between measurements of oscillations of neutrinos and anti-neutrinos. Poor knowledge of the cross-sections present one of the largest systematic errors limiting these analyses, and so a precise determination of these cross sections is vital to future measurements.

Another pion production process is the coherent neutrino-nucleus interaction. In this process the neutrino interacts off the entire nucleus, at very low momentum transfer, resulting in a forward-going pion and leaving the nucleus in the ground state. This process can occur via both the charged and neutral currents and from both neutrinos and anti-neutrinos. Neutral-current interactions, which result in a π^0 in the final state, are of particular interest for oscillation experiments investigating ν_e appearance as it forms a large part of the background. The process has been observed at high (greater than 5 GeV) neutrino energy [147] and agrees with the standard Rein-Seghal model [148] predictions, which are based on PCAC with pion dominance. However, in the $1-3$ GeV, the landscape becomes unclear as the available data are limited. Both MiniBooNE [149] and SciBooNE [123] have measured the neutral-current mode at an average neutrino energy of 0.8 GeV. The charged current mode is mode is more puzzling. Isospin symmetry implies that the charged current process should occur with twice the rate of the neutral-current process. However K2K [150] and SciBooNE [151] have reported no evidence for the charged-current coherent process. It is now becoming clear that it is not appropriate to continue

the high-energy theory down to lower energies, and that other models involving microscopic Δ dominance are more reliable [152, 153]. Testing these models requires data on a number of different types of target nuclei and over a range of neutrino energies. This is crucial since the contribution of this process to the ν_e backgrounds in the first oscillation probability maximum must be predicted accurately for the LBL experiments.

2.2.4 Differences in the energy-dependent cross sections of ν_μ- and ν_e-nucleus interactions

To determine the mass hierarchy of neutrinos and to search for CP-invariance violation in the neutrino sector, current and upcoming accelerator-based neutrino oscillation experiments like T2K [154] and NOvA [155] as well as future proposed experiments such as LBNE [103] and the Neutrino Factory [156] plan to make precision measurements of the neutrino flavour oscillations $\overset{(-)}{\nu}_\mu \rightarrow \overset{(-)}{\nu}_e$ or $\overset{(-)}{\nu}_e \rightarrow \overset{(-)}{\nu}_\mu$. An important factor in the ability to fit the difference in observed event rates between the near and far detectors will be an accurate understanding of the cross section of ν_μ- and ν_e-nucleus interactions. Uncertainties on differences in expected event rates due to differences between these cross-sections will contribute to experimental uncertainties in these flavour oscillation measurements.

There are obvious differences in the cross sections due to the difference in mass of the outgoing lepton. These can be calculated by including the—often neglected—lepton-mass term in the cross-section expression. Figure 2 (right) [157], shows this expected differences in the cross sections as a function of neutrino energy. Another such obvious calculable difference occurs because of radiative corrections. Radiative corrections from a particle of mass m are proportional to $\log(1/m)$, which implies a significant difference due to the μ to e mass difference [158]. This turns into a roughly 10% difference in the cross sections. In addition to these obvious differences, there are other more subtle differences due to the coupling of poorly-known or simply unknown form factors to the lepton tensor that reflect the differences in the outgoing lepton mass. These effects have been investigated in some detail [157] but must be probed experimentally.

Regarding nuclear effects, while there are no differences expected in the final-state interactions, there are expected differences of the initial reaction cross-sections between ν_μ- and ν_e-nucleus interactions. Since the lepton tensor, reflecting the mass of the outgoing lepton, couples to the hadron-response functions, there is a difference in nuclear effects at the interaction vertex due to the μ to e mass difference. The expected difference in the ν_μ- and ν_e-nucleus cross-section ratio is around 5% when using a spectral-function model [159] for the initial nucleon momentum compared to the relativistic Fermi gas model [107, 160]. There is another 5% difference expected for multi-nucleon (np-nh) contribution [161].

These differences in cross sections extend up into the resonance region with the low-Q^2 behaviour of Δ production exhibiting 10% differences at values of Q^2 where the cross section has levelled off.

While each of the above individual effects may not be large compared to current neutrino-interaction uncertainties, they are large compared to the assumed precision of oscillation sensitivity studies for the LBL programme. Moreover, the sum of these effects could be quite significant and the uncertainty in our knowledge of the size of these effects will contribute directly to uncertainties in the neutrino-oscillation parameters measured in these experiments—and these uncertainties can only be reduced with good quality ν_e scattering data. νSTORM is the only source of a well-understood and well-controlled ν_e neutrino beam with which to carefully study these cross section differences.

2.2.5 Effects of neutrino-nucleus interaction systematics on oscillation measurements

A neutrino-oscillation experiment must compare neutrino-scattering event rates with a prediction in order to extract oscillation parameters. Many systematic errors in such analyses can be mitigated by use of a near detector

with similar target nuclei, but, importantly, several systematic uncertainties still remain. Neutrino oscillation is a function of the true energy of the neutrino, but experiments must infer the energy of neutrino interactions from measurements of the outgoing charged-lepton partner (which also identifies the neutrino flavour).

As discussed in section 2.2.2, the problem we face is that the micro-physics of the nuclear environment can change the mapping between the charged-lepton momentum and the neutrino energy. This mapping is model-dependent because the form factors for axial-currents have not yet been measured precisely, due to the fact that uncertainty in the reconstructed neutrino energy is inherently wider than the widths of nuclear effects. The model-dependence of these predictions adds a systematic uncertainty that cannot be mitigated without data sets that are fine enough in final-state-particle resolution while covering enough of the kinematic phase space and target nuclei. We note that systematic uncertainty due to this model dependence cannot be mitigated by a near detector unless and until the model calculations are sufficiently detailed to allow falsification with final-state particle data. Another issue that contributes to the systematic errors is the migration of events between near (and far) detector data samples. Mainly these arise because final-state particles can scatter hadronically within the target nucleus before escaping into the detector medium. As discussed in section 2.2.3, the exact kinematics of the final-state particles in the resonance region must be predicted, and then measured, in order to reduce these uncertainties. Finally there is the very real effect of differences in the ν_μ and ν_e interaction cross sections, which must be measured with high precision.

The stated goals for the precision of the proposed next generation long-baseline neutrino oscillation experiments such as LBNE, LBNO, and T2HK cannot be reached without mitigating these systematic uncertainties, even with high precision near detectors. νSTORM is the only experimental facility with the precision and flexibility needed to tackle all of these neutrino interaction cross section uncertainties.

2.3 Technology test-bed

The muon storage ring similar to the proposed for the nuSTORM has never been used for neutrino beam production and neutrino physics experiments. The possibility to produce and exploit in experimental investigations the high quality neutrino beam based on muon decay is the most exciting aspect of this proposal.

Although a muon ring in such configuration has never been realised, the accelerator system of the proposed nuSTORM can be fully based on the existing and well tested technology currently in use in many laboratories around the world. The required proton beam of 100-200 kW power and 40-60 GeV can be produced using existing proton accelerators. In particular those parameters can be easily achieved using the SPS machine at CERN, although the details of the configuration, including the necessary alteration to the current operational setting remains to be studied including its effect on the beam quality in the main modes of the machine operation (as the LHC injector) . The target and pion collection system can be realised using the solid target technology and the magnetic horn. The mature operational knowledge for these technologies exist at CERN and was demonstrated numerous times including the CNGS operation in the even more difficult regime than the one required for the nuSTORM. The magnetic system for the pion/muon transport consists of the standard room temperature magnets, although with large aperture. Such magnets have been successfully built and operated for example for the MICE experiment at RAL or COMPASS at CERN. The decay ring magnets share similar need for large aperture for room temperature magnets in the neutrino production straight and either room temperature or superconducting magnets in the arc section, which will be decided based on the cost comparison. It is believed that those magnets including those for the FFAG ring option can be achieved based on current technology. The scaling FFAG has been successfully demonstrated at KURRI (Osaka, Japan), where an impressive chain of those type of rings has been constructed and is now in operation for the ADSR experiment. Also the section of the straight scaling FFAG, which is required for the production straights of the nuSTORM ring has been constructed and proven to behave in operation as expected [ref].

The instrumentation for the nuSTORM ring needs to be carefully considered. It must address the beam diagnostics for the machine operation, but also the monitoring of muon beam properties responsible for the quality of the neutrino beam production. The machine operation requires a precise beam position, profile and intensity measurements. They may be based on the existing BPM , beam profile and wall current monitors, although some care is needed due to a large muon beam emittance in the nuSTORM.

The production of the high quality neutrino beam requires in addition measuring the muon beam energy, energy spread, polarisation and divergence. By recording the spectrum and polarisation of electrons coming from the muon decay turn by turn downstream of the dipole magnet used as a spectrometer, the necessary information on the muon beam energy, energy spread and polarisation can be deduced. Several methods were proposed to measure muon beam divergence using Helium filled Cherenkov radiator, using optical transition radiation device or observing photons from radiative muon decay. The details of the muon beam monitoring remains to be addressed in future studies.

The use of the nuSTORM ring to generate a high quality muon beam for a future advanced ionisation cooling experiment after extracting the beam may be an interesting additional application with a potential important application for a future Higgs Factory or a Muon Collider.

3 The νSTORM facility; overview

3.1 Accelerator facility

The facility proposed would be based on the FODO lattice, race track shaped, muon decay ring described in the document: P.Kyberd et al. "nuSTORM: Neutrinos from STORed Muons" (arXiv:1206.0294). The ideas are summarised below.

The basic concept for the facility is presented in figure 4and the production part in figure **??**. A high-intensity proton source places beam on a target, producing a large spectrum of secondary pions. Forward pions are focused by a collection element into a transport channel. Pions decay within the first straight of the decay ring and a fraction of the resulting muons are stored in the ring. Muon decay within the straight sections will produce neutrino beams of known flux and flavour via: $\mu^+ \to e^+ \nu_e \bar{\nu}_\mu$ or $\mu^- \to e^- \bar{\nu}_e \nu_\mu$. A storage ring of 3.8 GeV/c is proposed to obtain the desired spectrum of ~ 2 GeV neutrinos; pions have then to be captured at a momentum of approximately 5 GeV/c. An overview of the parameters is shown in table 1.

3.1.1 Production

The production part of the facility is shown in figure 2 (could we instead of this get a sketch showing the layout with all distances up to the injection point so that we can lay it out at CERN).

Simulations using a gold target show that the flux of neutrinos would be comparable to (arXiv:1206.0294):

$$N_\mu = \mathrm{POT} \times (\pi \text{ per POT}) \times \epsilon_{\mathrm{col}} \times \epsilon_{\mathrm{trans}} \times \epsilon_{\mathrm{inj}} \times (\mu \text{ per } \pi) \times \mathrm{Adyn} \times \Omega \tag{1}$$

where POT is the number of protons on target, ϵ_{col} is the collection efficiency, $\epsilon_{\mathrm{trans}}$ is the transport efficiency, ϵ_{inj} is the injection efficiency, μ per π is the chance that an injected pion results in a muon within the ring acceptance, Adyn is the probability that a muon within the decay ring aperture is within the dynamic aperture, and Ω is the fraction of the ring circumference that directs muons at the far detector. νSTORM assumes 10^{21} POT for a 4–5 year run using 60 GeV protons. From arXiv:1206.0294, one obtains (with horn collection) $\sim 0.1\pi/POT \times \text{collection efficiency}$. The collection efficiency is 0.8. The transport efficiency, and the injection efficiency are assumed as 0.8 and 0.9, respectively and that the probability that a π decay results in a

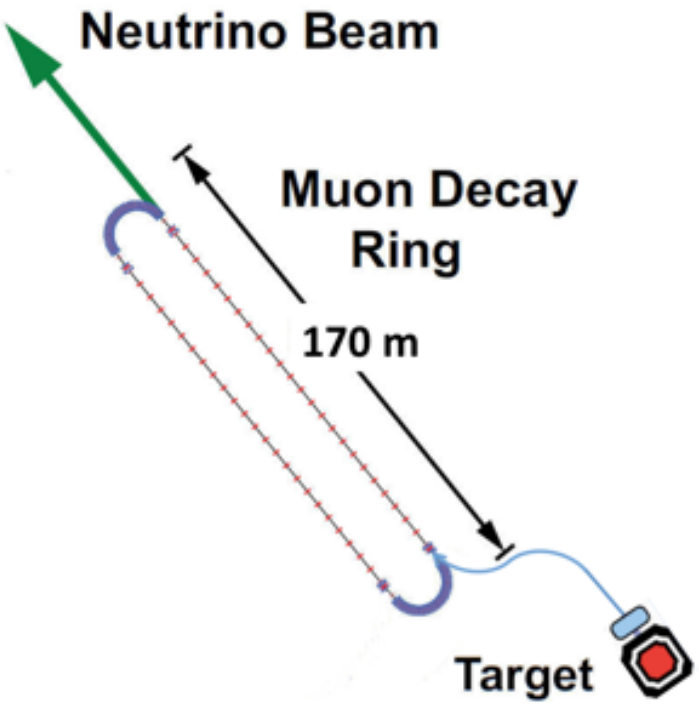

Figure 4: The nuSTORM facility, 150 m straights and 25m 180 degree arcs.

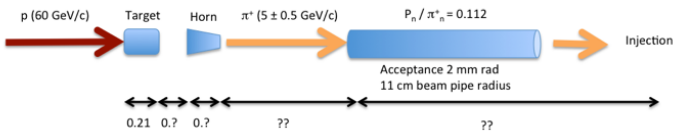

Figure 5: The production part layout of the nuSTORM facility.

Table 1: Summary of parameters for nuStorm and CERN, differences are marked in bold, indented fonts. **(Some parameters of CERN have been taken from the NESSiE proposal this has to be corrected if necessary)**.

Neutrino characteristics	**Fermilab**	**CERN**
Aimed neutrino energy [GeV]	1.0 to 3.0	1.0 to 3.0
Flux measurement precision [%]	1.0	1.0
Protons on target (POT)	1021	2.3 1020
Useful μ decays $[10^{18}]$	1.00	$100/60 = 1.67$
Production, horn and injection		
Target diameter/length [m], material	?/0.21	?/21
Pulse length [μs]	?	10.5
Proton energy [GeV/c]	60	100
Beam Size, σ [m] On target?	?	5.3 10-4
Pion energy [GeV/c]	$5.0 \pm 10\%$	$5.0 \pm 10\%$
Horn diameter/length [m]	?	0.16 / 0.40
Reflector diameter/length [m]	?	0.16 / 0.39
Current Horn/Reflector [kA]	300	300/150
Estimated collection efficiency	0.8	0.8
Estimated transport efficiency	0.8	0.8
Estimated injection efficiency	0.9	0.9
Acceptance [mm rad]	2.0	2.0
π/pot within momentum acceptance	0.112 ???	$0.112 \times \frac{100}{60} = 0.187$
Length of target [m]	0.21	0.21
Distance between target and horn [m]	?	
Length of horn [m]	?	
Distance between horn and injection [m]	?	
The muon storage ring		
Momentum of circulating muon beam [GeV/c]	3.8	3.8
Momentum of circulating pion beam [GeV/c]	$5.0 \pm 10\%$	$5.0 \pm 10\%$
Circumference [m]	350	350
Length of straight [m]	150	150
Ratio of Lstraight to ring circumference [Ω]	0.43	0.43
Dynamic aperture, Adyn	0.7	0.7
Acceptance [mm rad]	2.0	2.0
Decay length [m]	240	240
Fraction of π decaying in straight (Fs)	0.41	0.41
Relative μ yield [p15/p37] ($\mathrm{Adyn} \times (\pi \text{ per POT}) \times \mathrm{Fs} \times \Omega$)	0.014	
Detectors		
Distance from target [m]		300/1600

μ within the acceptance time $\gamma c\tau$ is 0.08. Ω is 0.34 (this is not consistent with the table above, different values found in arXiv:1206.0294, 0.34 and 0.43 is this a typo or another version of the ring).

The number of pions produced off various targets by 60 GeV/c protons has been simulated [arXiv:1206.0294]. Target optimisation based on a conservative estimate for the decay-ring acceptance of 2 mm-radian corresponds to a decay ring with 11 cm internal radius and a function of 600 cm. The optimal target length depends on the target material and the secondary pion momentum. Results of the optimisation study are presented in Table I. Approximately 0.11 π/POT can be collected into a $\pm 10\%$ momentum acceptance off medium/heavy targets assuming ideal capture.

For example, with a NuMI-like horn operating at 300 kA and using a 22 cm gold target, it is possible to collect 0.088 π/POT within a momentum band of 5 ± 0.5 GeV/c. Optimisation of the horn inner shape could increase the number of For example, collected pions. Where do the figures come from?? I For example, cannot deduce them from tables or text.

For the CERN implementation (100 GeV proton case) the simulation For example, studies show that the μ/POT is linear with energy.

The feasibility of the target, to make the final material and mechanical choices would also need following studies:

1. Heat removal. A significant heat load is deposited by the beam on the target and has to be removed reliably by the cooling system.
2. Static and dynamic stresses. The target must withstand thermal-mechanical stresses arising from the beam induced heating of the target.
3. Radiation damage. Degradation of the material properties due to radiation damage must be accommodated.
4. Geometrical constraints. The target has to fit inside the bore of the magnetic horn whilst having an appropriate geometry for effective pion production.
5. Remote replacement. Once activated the target has to be remotely manipulated in the event of failure.
6. Minimum expected lifetime. The target is expected operate without intervention between scheduled maintenance shutdowns.
7. Safe operation. The target design should minimise any hazard to the personnel or the environment

The beam structure below μs can not be "seen" by the target. The beam pulse has to be fast extracted.

3.1.2 Injection (no change for CERN)

Pion decay within the ring, and non-Liouvillean "stochastic injection" is assumed to be an optimised option. In stochastic injection, the $\simeq 5$ GeV/c pion beam is transported from the target into the storage ring and dispersion-matched into a long straight section. Circulating and injection orbits are separated by momentum. Decays within that straight section provide muons that are within the $\simeq 3.8$ GeV/c ring momentum acceptance. With stochastic injection, muons from a beam pulse as long as the FNAL Main Injector circumference (3 000 m) can be accumulated, and no injection kickers are needed, see figure 6. Note: for 5.0 GeV/c pions, the decay length is $\simeq 280$ m; $\simeq 42\%$ decay within the 150 m decay ring straight.

3.1.3 Decay ring (no change for CERN)

The Decay Ring ring is a compact racetrack ring design based on separate function magnets. The design goal is to maximise the momentum acceptance (around 3.8 GeV/c central momentum), while maintaining reasonable physical apertures for the magnets in order to keep the cost down. This is accomplished by employing strongly

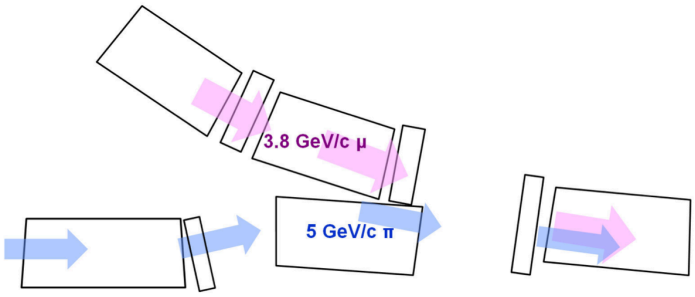

Figure 6: Stochastic injection.

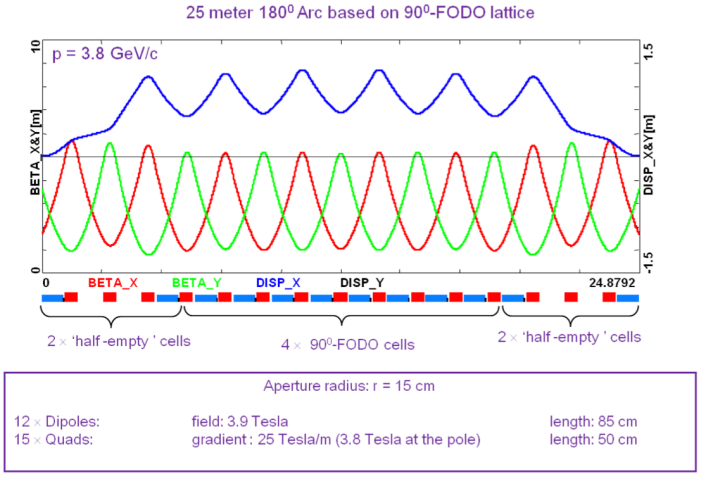

Figure 7: The arc lattice and magnets.

focusing optics in the arcs (90° phase advance per FODO cell), featuring small β functions ($\simeq$ 3 m average) and low dispersion ($\simeq$ 0.8 m average). The linear optics for one of the 180-degree arcs is illustrated in figure 7.

The current lattice design incorporates a missing-magnet dispersion suppressor. The missing-magnet dispersion suppressor will house the stochastic injection. With a dispersion of $\eta \simeq 1.2$ m at the drift, the 5 GeV/c and 3.8 GeV/c orbits are separated by $\simeq 30$ cm; an aperture of $\simeq \pm 15$ cm is available for both the 5 GeV/c π and 3.8 GeV/c μ orbits. To maintain high compactness of the arc, while accommodating adequate drift space for the injection chicane to merge, two special "half empty" cells with only one dipole per cell were inserted at both arc ends to suppress the horizontal dispersion. This solution will limit the overall arc length to about 25 m, while keeping the dipole fields below 4 T. The arc magnets assume a relatively small physical aperture radius of 15 cm, which limits the maximum field at the quadrupole magnet pole tip to less than 4 T.

On the other hand, the decay straight section requires much larger values of β-functions ($\simeq$ 40 m average) in order to maintain small beam divergence ($\simeq$ 7 mrad). The resulting muon beam divergence is a factor of 4 smaller than the characteristic decay cone of $1/\gamma$ ($\simeq 0.028$ at 3.8 GeV). As illustrated in figure **??**, the decay straight is configured with a much weaker focusing FODO lattice (30° phase advance per cell). It uses normal conducting large aperture (r = 30 cm) quads with a modest gradient of 1.1 T/m (0.4 T at the pole tip). Both the arc and the straight are smoothly matched via a compact telescope insert, as illustrated in figure **??**.

The "other" 150 m straight, which is not used for neutrino production, can be designed using much tighter FODO lattice (60° phase advance per cell), with rather small β functions comparable to the one in the arc

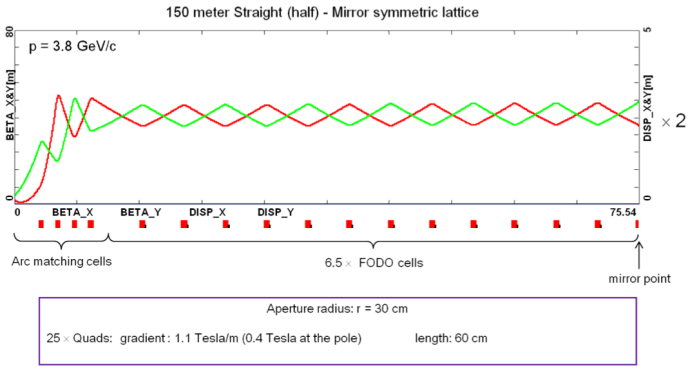

Figure 8: The decay straight section.

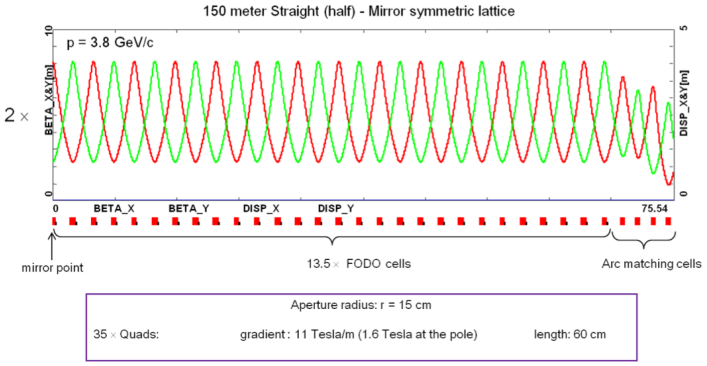

Figure 9: The other decay straight section.

($\simeq$ 5 m average). This way one can restrict the aperture radius of the straight to 15 cm. Again, the second straight uses normal conducting, quads with a gradient of 11 T/m (1.6 T at the pole tip). Both the arc and the straight are smoothly matched, as illustrated in figure **??**.

Finally, the complete racetrack ring architecture features the "low-β" straight (half) matched to the 180° arc and followed by the high-β decay straight (half) connected to the arc with a compact telescope insert. To summarise the magnet requirements, both 180° arcs were configured with 3.9 T dipoles and 25 T/m quads (superconducting magnets with 15 cm aperture radius).

Both straights use normal conducting magnets: the decay straight, 1.1 T/m quads with 30 cm aperture radius and the other straight, 11 T/m quads with 15 cm aperture radius. These magnets have challenging apertures.

The transverse normalised acceptance of the ring is 78 mm rad both in x and y (or geometric acceptance of 2.1 mm rad) for the net momentum acceptance of $\pm 10\%$.

3.2 Detectors for sterile neutrino search

The Super B Iron Neutrino Detector (SuperBIND), an iron and scintillator sampling calorimeter similar in concept to the MINOS detector, is assumed as the baseline detector for the sterile-neutrino search focusing on muon-neutrino appearance and disappearance searches. Two detectors of this type would be used for short baseline oscillation measurements; one 100 Ton detector at 50 m and a 1.6 kTon detector 2 km from the storage ring. The near detector is required to measure the characteristics of the neutrino beam prior to oscillation for the reduction of systematic uncertainties. Simulations have been conducted for the far detector — a near detector

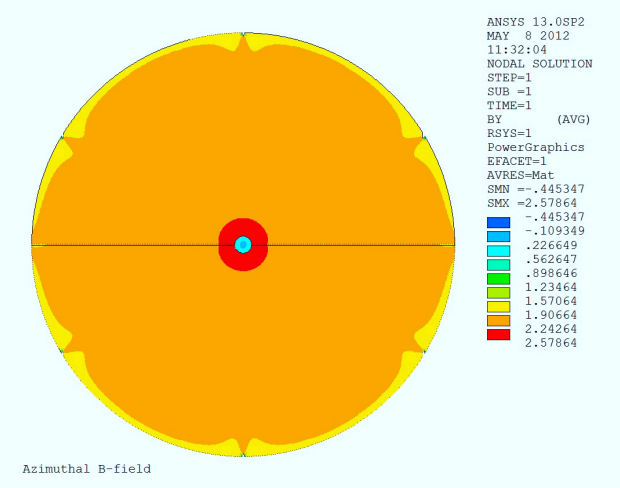

Figure 10: A 2-D finite element magnetic field simulation of the SuperBIND iron plate.

simulation is in preparation.

The far detector has a circular cross-section 5 m in diameter. The iron planes are to be 2 cm in depth and constructed from two semi-circular pieces skip welded at a central join. The detector is magnetised using multiple turns of a superconducting transmission line (STL) [162] to carry a total of 250 kA to induce a magnetic field between 1.5 T and 2.5 T within the iron plate. To accommodate the STL, a 20 cm bore runs through the centre of the detector. A 2-D finite element magnetic field analysis of the iron plate has been performed, with the results shown in figure 10.

The scintillator detector planes are composed of two layers of $1\times1\,\mathrm{cm}^2$ scintillating bars providing vertical and horizontal readouts at each detection plane. A 1 mm bore through the centre of each bar is provided for the insertion of a wavelength shifting fibre. Each scintillator bar is read out from both ends using silicon photo-multipliers.

3.2.1 Far Detector Simulation

A detailed detector simulation and reconstruction exists for the determination of the detector response. The simulation was based on software developed for the Neutrino Factory Magnetised Iron Neutrino Detector (MIND) [163]. Neutrino event generation is accomplished through the use of the GENIE [164] event generator. Events are passed to a GEANT4-based [165] simulation for the propagation of the final-state particles through successive steel and scintillator layers. This simulation includes hadron interactions simulated by the QGSP_BERT physics list [165]. Hits in the scintillator are grouped into clusters, smearing the detector hit position, and energy deposition of the accumulated hits is attenuated in a simple digitisation algorithm applied prior to reconstruction.

Magnetisation within the iron is introduced by reducing the model of figure 10 to a toroidal magnetic field with a radial dependence which follows the expression:

$$B_\phi(r) = B_0 + \frac{B_1}{r} + B_2 e^{-Hr}\,; \tag{2}$$

where $B_0 = 1.53\,\mathrm{T}$, $B_1 = 0.032\,\mathrm{T\,m}$, $B_2 = 0.64\,\mathrm{T}$, and $H = 0.28\,\mathrm{m}^{-1}$. This parameterisation and the field along the 45° azimuthal direction are shown in fugure 11.

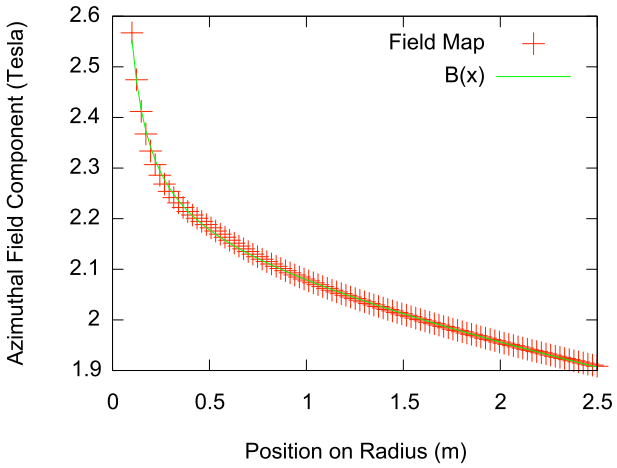

Figure 11: The magnetic field magnitude as a function of radius along the 45° azimuth with the parameterisation used in the detector simulation.

Table 2: The fraction of events left but cuts applied to simulations of the indicated species in the nominal SuperBIND detector when the appearance of a μ^- in an event is defined as the experimental signal.

	Interaction Type and Species				
Event Cut	ν_μ CC(%)	$\bar{\nu}_\mu$ CC ($\times 10^3$)	ν_e CC ($\times 10^3$)	$\bar{\nu}_\mu$ NC ($\times 10^3$)	$\bar{\nu}_e$ NC ($\times 10^3$)
Successful Reconstruction	71.6%	27.8	236	55.0	77.8
Fiducial	68.9%	22.5	227	53.0	74.6
Maximum Momentum	68.0%	17.6	201	46.4	65.6
Fitted Proportion	67.6%	16.8	192	44.7	63.2
Track Quality	59.5%	4.8	36.1	10.5	15.4
NC Rejection	25.2%	0.07	0.0	0.005	0.005

The reconstruction uses multiple passes of a Kalman filtering and fitting algorithm for the purposes of identifying muon trajectories within events and to determine the momentum and charge for an identified track. The algorithms are supplied by the RecPack software package [166]. Geometrical information from the track including: the extent of the track; the direction of bending in the magnetic field; and the pitch of the track are used at various points in this procedure to provide information to the Kalman filter. The hadron reconstruction is not yet well developed so the neutrino energy is reconstructed either by using the quasi-elastic approximation, if no hadronization is visible, or by smearing the true hadron energy according to the results of the MINOS CalDet test beam [167].

3.2.2 Event Selection

The selection of events is achieved by applying the sequence of cuts shown in table 2. The majority of these cuts are made to ensure that the trajectory fit is of good quality. Cuts are made to remove events that are not successfully reconstructed, with a starting position closer than 1 m from the end of the detector. The fit to the muon trajectory is also required to produce a momentum less than 1.6 times the maximum neutrino energy, and must involve more than 60% of all detector hits assigned to be part of the trajectory.

Two further cuts—the track quality and NC rejection cuts—affect the ratio of signal to background. The

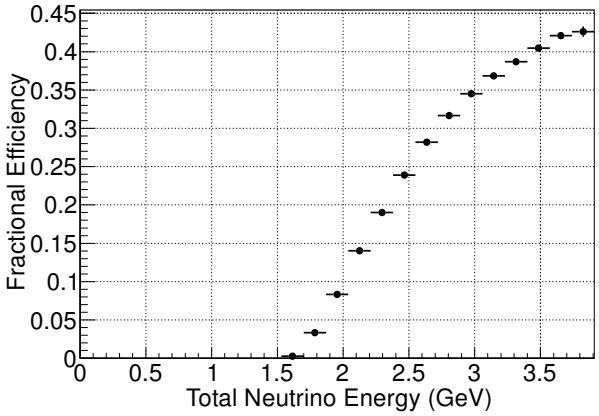

Figure 12: Efficiency of detection of a μ^- signal for a sample of ν_μ Charge Current interactions stopping in a SuperBIND detector.

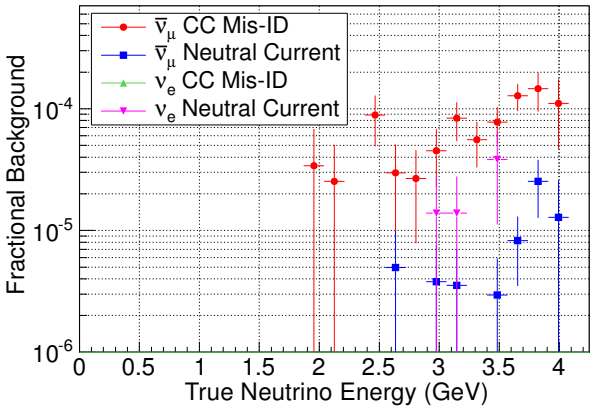

Figure 13: Backgrounds for the detection of a μ^- signal that will be present when μ^+ are contained in the νSTORM storage ring.

track quality cut is based on the relative error of the inverse momentum of the candidate muon $|\sigma_{q/p}/(q/p)|$ where q is the charge of the muon and p is its momentum. Probability distribution functions, $P(\sigma_{q/p}/(q/p))$, are generated from pure charged current (CC) and neutral current (NC) samples. A log-likelihood ratio, $\mathcal{L}_{q/p}$, is created from the ratio of the CC and NC probabilities for a given trajectory:

$$\mathcal{L}_{q/p} = \log\left(\frac{P(\sigma_{q/p}/(q/p)|CC)}{P(\sigma_{q/p}/(q/p)|NC)}\right) . \tag{3}$$

An event passes this cut if $\mathcal{L}_{q/p} > -0.5$. The NC rejection cut is likewise defined using a log-likelihood ratio of probability distribution functions defined using the number of hits used in a fit to a particular trajectory, N_{hit}, for CC and NC samples. It has found that the background rejection can be reduced to below parts in 10^{-4} if:

$$\mathcal{L}_{CC} = \log\left(\frac{P(N_{hit}|CC)}{P(N_{hit}|NC)}\right) > 6.5 . \tag{4}$$

The signal and background efficiencies are shown in figures 12 and 13, respectively.

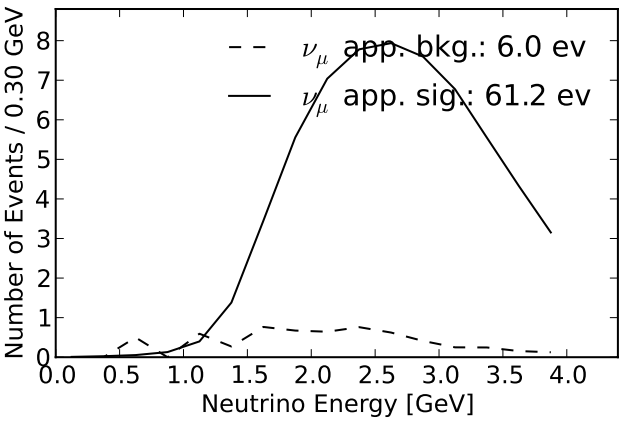

Figure 14: The neutrino spectrum measured at the SuperBIND far detector using the simulated detector response.

3.2.3 Sensitivities

Appearance physics via the channel $\nu_e \rightarrow \nu_\mu$ gives νSTORM broad sensitivity to sterile neutrinos and directly tests the LSND/MiniBooNE anomaly. The oscillation probabilities for both appearance and disappearance physics are:

$$P_{\nu_e \rightarrow \nu_\mu} = 4|U_{e4}|^2|U_{\mu 4}|^2 \sin^2\left(\frac{\Delta m^2_{41} L}{4E}\right) \text{ ; and} \quad (5)$$

$$P_{\nu_\alpha \rightarrow \nu_\alpha} = 1 - [4|U_{\alpha 4}|^2(1-|U_{\alpha 4}|^2)] \sin^2\left(\frac{\Delta m^2_{41} L}{4E}\right) . \quad (6)$$

The detector is designed for the appearance signal $\nu_e \rightarrow \nu_\mu$; the CPT conjugate of the channel with which LSND observed an anomaly, $\bar{\nu}_\mu \rightarrow \bar{\nu}_e$. Although it is clear from equation 5 that the appearance channel is doubly suppressed relative to the disappearance channel, the experiment is much more sensitive to the appearance channel due to better suppression of backgrounds for wrong-sign muon searches.

The detector response derived from simulation is used to determine the sensitivity of the experiment to potential sterile neutrinos. The detector response is summarised as a "migration" matrix of the probability that a neutrino generated at in a particular energy bin i is reconstructed in energy bin j. Defined in this way, the migration matrix encapsulates both the resolution of the detector and its efficiency. Samples of all neutrino interactions that could participate in the experiment are generated to determine the response for each detection channel. The spectrum of expected signal and background for this simulation is shown in figure 14 assuming 1.8×10^{18} μ^+ decays collected over 5 years. A contour plot showing the sensitivity of the experiment to the appearance of sterile neutrinos is shown in figure 15. These contours are shown with respect to the derived variable $\sin^2 2\theta_{e\mu} = |U_{e4}|^2|U_{\mu 4}|^2$. This contour, generated assuming only statistical uncertainties, shows that the appearance channel alone has the sensitivity to probe the LSND anomaly at 10σ confidence level.

3.3 Detectors for neutrino scattering studies

3.3.1 HIRESMNU: A High Resolution Near Detector à la LBNE

Precision measurements of neutrino-interactions at the near-detector (ND) are necessary to ensure the highest possible sensitivity to the neutrino oscillation studies in this proposal. Regardless of the process under study—

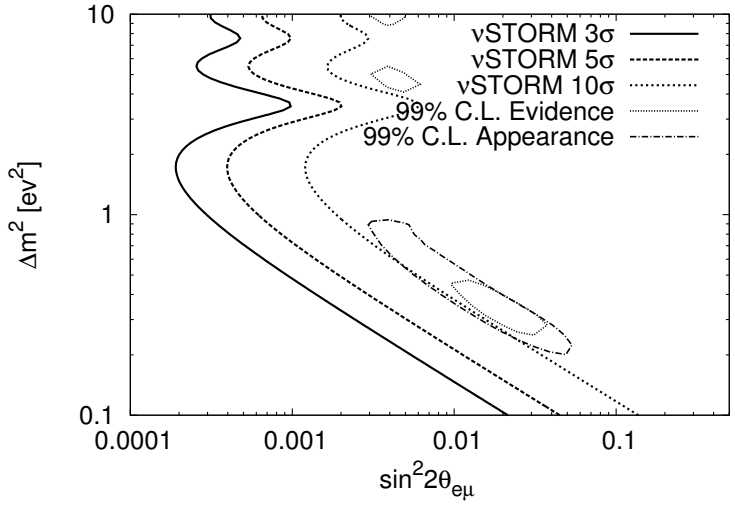

Figure 15: Statistics only contours of the χ^2 deviation from the no-sterile neutrino hypothesis corresponding to 3σ ($\chi^2 = 9$), $5\sigma(\chi^2 = 25)$ and $10\sigma(\chi^2 = 100)$ overlaid with 99% confidence level contours from experiments showing evidence for unknown signals and contours derived from the accumulated data from all applicable neutrino appearance experiments, as described in Fig.1.

$\boldsymbol{\nu_\mu \to \nu_e}$ ($\boldsymbol{\bar{\nu}_\mu \to \bar{\nu}_e}$) appearance or $\boldsymbol{\nu_\mu}$ ($\boldsymbol{\bar{\nu}_\mu}$) disappearance—the systematic error should be less than the corresponding statistical error. The ND must fulfill the following four principal goals:

- Measurement of the absolute and the relative abundance of the four species of neutrinos, $\boldsymbol{\nu_\mu}$, $\boldsymbol{\bar{\nu}_\mu}$, $\boldsymbol{\nu_e}$, and $\boldsymbol{\bar{\nu}_e}$, as a function of energy ($\boldsymbol{E_\nu}$). Accurate determination of the angle and the momentum of the electron in neutrino-electron neutral current interaction will provide the absolute flux;
- Determination of the absolute $\boldsymbol{E_\nu}$-scale, a factor which determines value of the oscillation-parameter Δm^2;
- Measurement of $\boldsymbol{\pi^0}$'s and of $\boldsymbol{\pi^+}$ and $\boldsymbol{\pi^-}$ produced in the NC and CC interactions. The pions are the predominant source of background for any oscillation study; and
- Measurement of ν-Nucleus cross-section where the nuclear target will be that of the far-detector. The cross-section measurements of exclusive and inclusive CC and NC processes will furnish a rich panoply of physics relevant for most neutrino research. Knowing the cross sections at the $\boldsymbol{E_\nu}$ typical of the νSTORM beam is essential for predicting both the signal and the background.

A near detector concept which will well meet these four requirements is a high resolution detector, the HIRESMNU, which has been proposed as the ND for the LBNE project [**?**]. Figure 16 shows a schematic of this the HIRESMNU design. The architecture of the detector [**?**] builds upon the experience of NOMAD [**?**]. It embeds a $4 \times 4 \times 7\,\mathrm{m}^3$ STT, surrounded by a 4π electromagnetic calorimeter (ECAL) in a dipole magnet with $B \simeq 0.4\,\mathrm{T}$. Downstream of the magnet and within the magnet yoke are detectors for muon identification. The STT will have a low average density similar to liquid hydrogen, about $0.1\,\mathrm{gm/cm}^3$, which is essential for the momentum determination and ID of electrons, protons, and pions. The foil layers, up and downstream of the straw tubes, provide the transition-radiation and constitute most of the 7 ton fiducial mass. The foil layers serve both as the mass on which the neutrinos will interact and as generators of transition radiation (TR), which provides electron identification.

Along the beam, the total depth of the detector, in radiation lengths, is sufficient for 50% of the photons, largely from the $\boldsymbol{\pi^0}$ decay, to be observed as e^+e^- pairs, which delivers superior resolution compared with conversions in the ECAL. Layers of nuclear-targets will be deployed at the upstream end of the STT for the

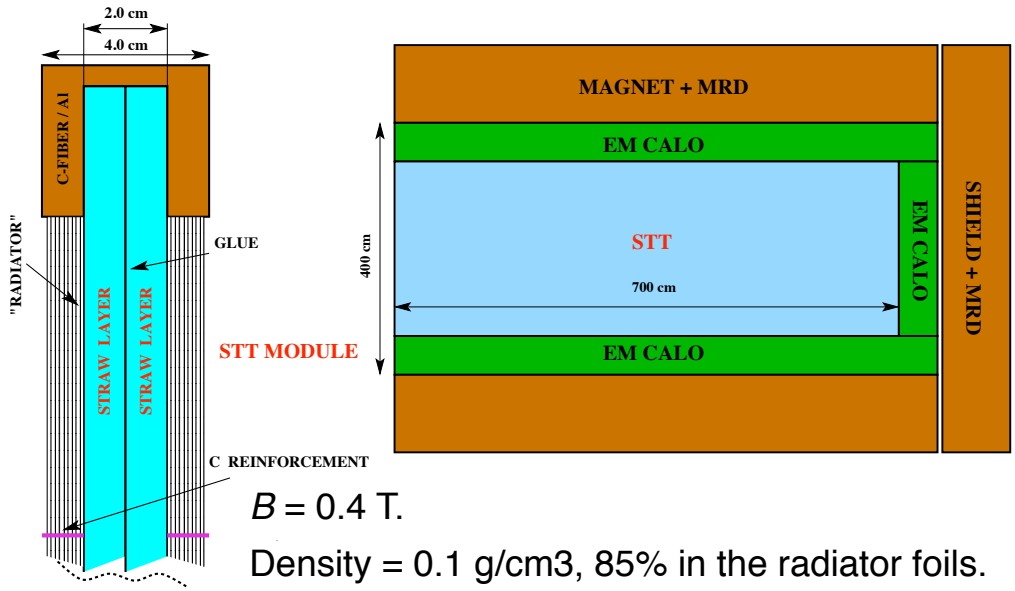

Figure 16: Schematic of the ND showing the straw tube tracker (STT), the electromagnetic calorimeter (ECAL) and the magnet with the muon range detector (MRD). The STT is based upon ATLAS [**?**] and COMPASS [**?**] trackers. Also shown is one module of the proposed straw tube tracker (STT). Interleaved with the straw tube layers are plastic foil radiators, which provide 85% of the mass of the STT. At the upstream end of the STT are layers of nuclear-target for the measurement of cross sections and the π^0's on these materials.

determination of cross sections on these materials.

The HIRESMNU delivers powerful sensitive systematic constraints on neutrino cross-section of exclusive and inclusive processes, on the multiplicity of secondary particles produced in neutrino interactions, and on characterizing the neutrino source. It can identify all four neutrino species in νSTORM. The studies have been done within the LBNE context. The systematic studies include ν-electron scattering, quasi-elastic interactions, $\nu_e/\bar{\nu}_e$-CC, neutral-current identification, π^0 detection, etc. The quoted dimensions, mass, and segmentation of HIRESMNU will be further optimized for νSTORM as the proposal evolves.

Physics topics offered by a high resolution detector such as HIRESMNU in NuStorm are summarized in Appendix A.

4 Implementing the νSTORM facility

In concept the following sections explain the implementation of nuSTORM at the respective laboratory. The "FNAL" section should have a section which presents what European/CERN contributions could be. The "CERN" section might include a complementary section.

4.1 Implementing νSTORM at CERN

The facility could be implemented in the SPS North Area, LSS2. Fast extraction from the SPS in the North Area, can be done by using an injection kicker in the LSS1 and extraction via an existing septum. For low intensities this has been tested, see figure 17.

The machine would ideally run after the LS2 upgrades of the injectors, including the new Linac4, see figure 18.

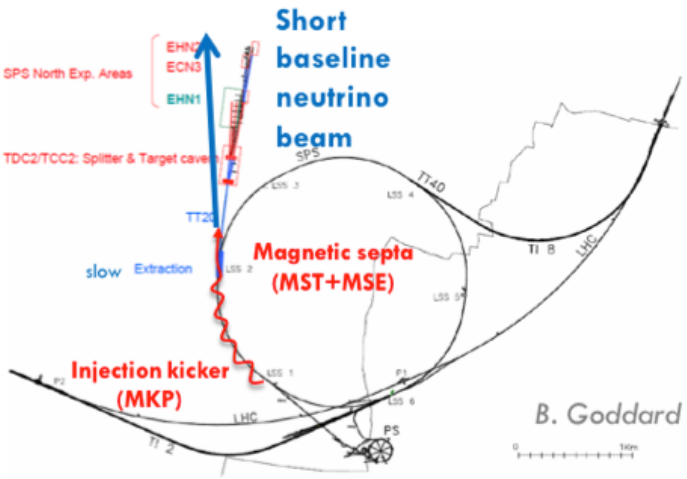

Figure 17: Extraction of the SPS beam in the North Area.

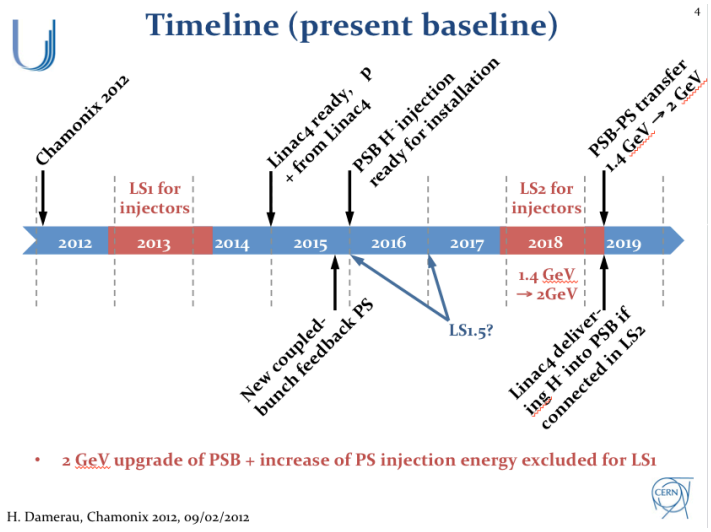

Figure 18: Timeline for the CERN injector upgrades.

Table 3: Summary of the SPS beam characteristics at present and after the LS2 upgrade.

Parameter	**SPS operation**		**SPS record**		**After LIU 2020**	
	LHC	CNGS	LHC	CNGS	LHC	CNGS/νSTORM
Energy [GeV]	450	400	450	400	450	400/100
Bunch spacing [ns]	50	5	25	5	25	5
Bunch intensity [1011]	1.6	0.105	1.3	0.13	2.2	0.17
Number of bunches	144	4200	288	4200	288	4200
SPS intensity [1013]	2.3	4.4	3.75	5.3	6.35	7.0
PS intensity [1013]	0.6	2.3	1.0	3.0	1.75	4.0
SPS Cycle length [s]	21.6	6.0	21.6	6.0	21.6	6.0/7.2 ??
PS Cycle length [s]	3.6	1.2	3.6	1.2	3.6	1.2/2.4
PS beam mom. [GeV/c]	26	14	26	14	26	14
Beam Power [kW]	77	470	125	565	211	747/622 (divide by 4) ??

SPS operation after LS2 upgrades can give up to 750 kW (7.0×10^{13} protons at 400 GeV every 3.6 s cycle). Operation at 3.6/6s? Is this feasible in PS-transition x-ing?

For nuSTORM a 100 GeV beam from the SPS is assumed. For 6 s cycling we would get 100 GeV * 7×10^{13} / 6 * 10^{-3} = 115 kW. As in the present CNGS facility, for fast proton extraction, the neutrino pulse duration will be 10.5 μs. The beam size would be $\sigma = 0.53$ mm (At extraction?. What about the target?).

What are the options when L4 is there?

In table 3 (from CERN EDMS1233951) the beam characteristics for the SPS before and after the LS2 upgrades are shown. Change 400 GeV to 100 GeV!

4.5×10^{19} pot/y is assumed as a conservative reference. What is this in terms of power out of the SPS?

If νSTORM would run for 5 years at 100 GeV protons, this corresponds to 5 * 4.5×10^{19} = 2.3×10^{20} pot for 5 years. However the π/pot is proportional to the energy, so we would be only a factor of 2 off. 10^{21} POT needed for νSTORM for 60 GeV protons in 4 to 5 years.

Should we use LAr detectors? Can the NESSiE detectors be used if they are put at CERN?

The same design of the extraction lines to the as NESSiE target is assumed. The target would be 60 m below surface (SPS extraction). A preliminary design of a Ta target for νSTORM has to be developed ... Au would melt?

If nuSTORM is going to run after NESSiE, one has to see if a new target station is needed or how re-furbish the existing. Is it possible to refurbish the target station at all?

What are the detectors we need? At what distance? Does this depend on the proton energy (100 and not 60 GeV)? NESSiE graphite target simple design exists. Design experience from NBI colleagues will be precious, considering feedback from running installations (T2K/NuMI/NoVA).

Beam 1sigma on target: 1-2.5 mm, divergence $\leq$ 1 mrad (maybe not the same meaning for νSTORM). How is this consistent with 0.53 mm above?

Layout:

Detector positions 20, 50 and 2000 m respectively (can the positions/detectors for NESSiE be used and would this be an advantage, presently they are at: 330, 1100 and 1600 m).

Below NESSiE option to be discussed for nuSTORM.

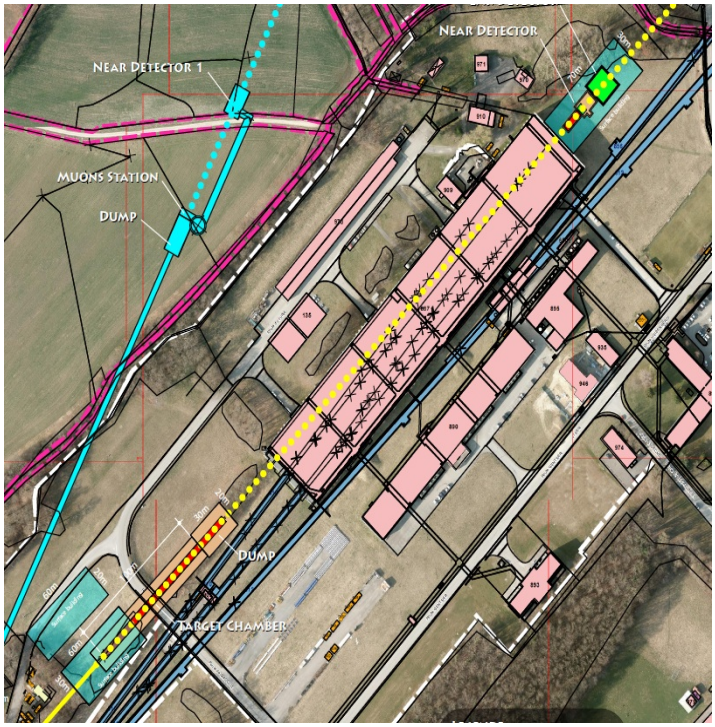

Figure 19: nuSTORM/NESSiE.

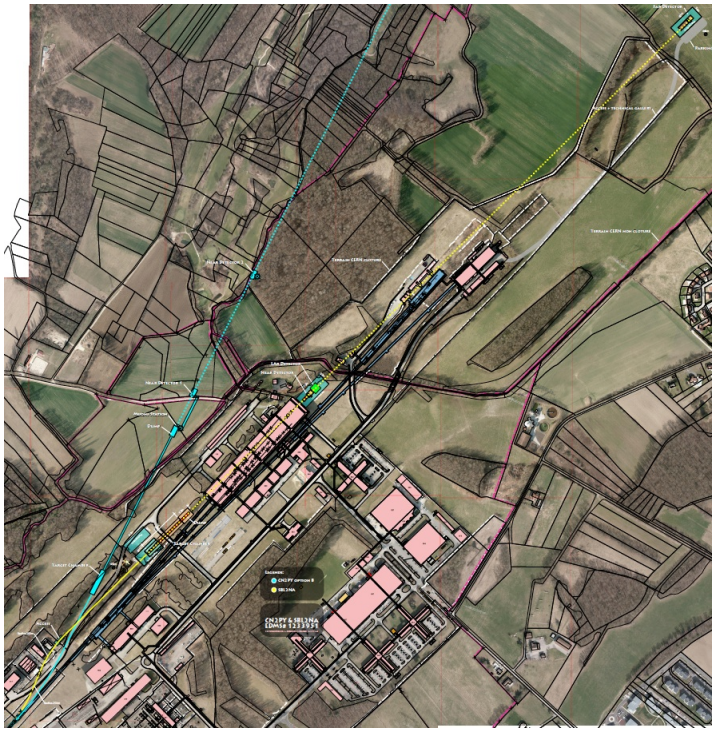

Figure 20: Far detector outside CERN fences.

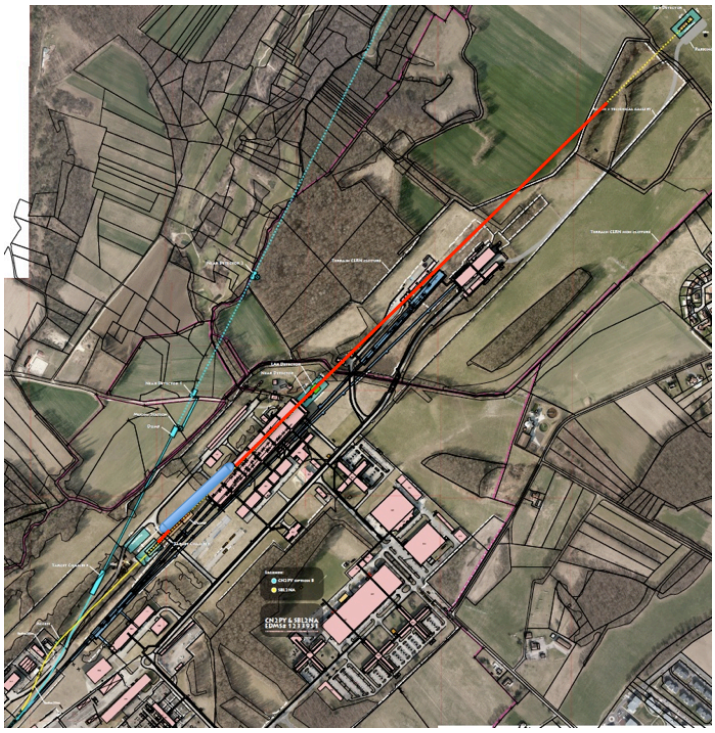

Figure 21: Another option.

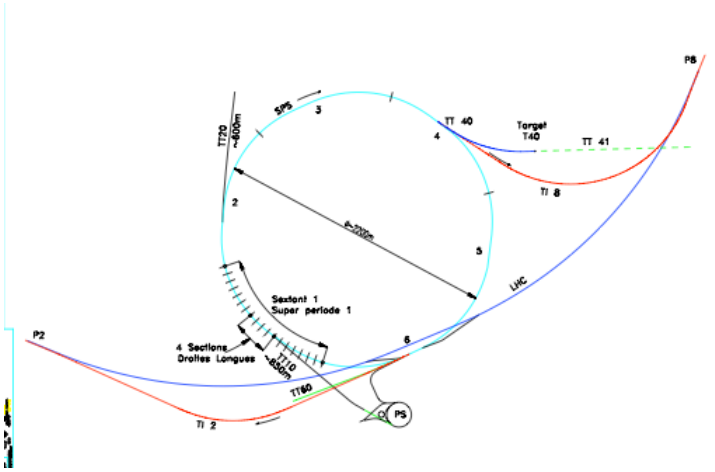

Figure 22: Another option.

4.2 Implementing νSTORM at FNAL

The concept for siting nuSTORM at Fermilab follows ideas that were developed nearly two decades ago for a short baseline $\nu_\mu \rightarrow \nu_\tau$ oscillation experiment [168, 169] that was to use protons extracted from the Fermilab Main Injector utilizing the proton abort line of that machine. Although this experiment was never carried out, the Main Injector abort beam absorber was assembled with the by-pass beam pipe that would have been needed for this experimnet. nuSTORM will utilize this by-pass. The basic siting concept for nuSTORM at Fermilab is shown in Fig. 23 Protons from the Fermilab Main Injector will be brought to a new target station located near

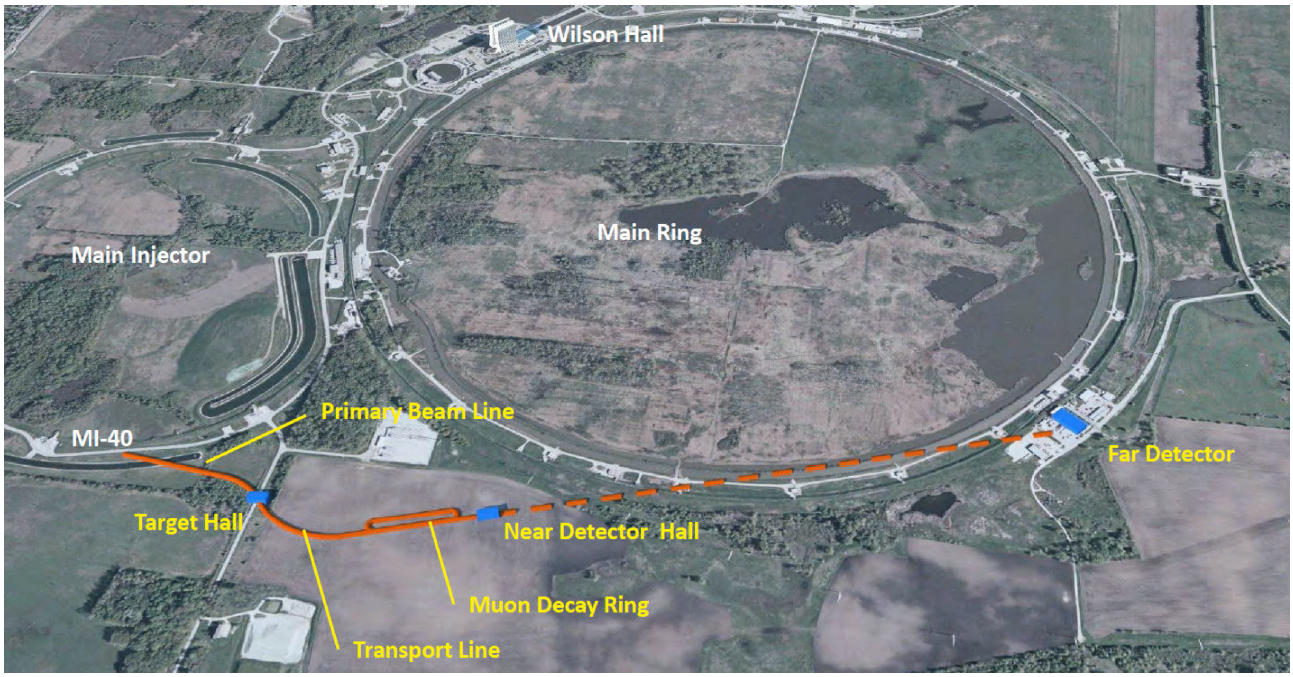

Figure 23: Schematic of the facility

the Southern edge of the Fermilab site. The beam line will be designed for 120 GeV protons, but the beam line will be able to accommodate protons from 60 to 120 GeV. Although the pion yield per proton on target increases linearly in the 60 to 120 GeV proton energy range, the run conditions for nuSTORM will have to take into consideration the other experiments running at the time. A detail of the current favored siting option for beam line, target hall, transport line and decay ring is shown in Fig. 24. For nuSTORM at Fermilab, the baseline in 100 kW on target which represents approximately 1/7 of the 700 kW total power available after completion of the Fermilab Proton Improvement Plan [170]. Current simulations for nuSTORM at Fermilab have assumed a Ta target and a NuMI-like horn operating at 300 kA. A schematic of the current target station concept in given in Fig. 25. The pion capture and transport line starts 30 cm downstream of the horn and transport pion to the decay ring. It is tuned to collect pions in the momentum acceptance of 5 $\pm$ 0.5 GeV/c. "Stocastic injection" (where the pions are injected into the ring on an orbit separated from the circulating muons) is used. The current design for the injection section is shown in Fig. 26. The decay ring is approximately 350 m in circumference and utilizes compact arcs. The ratio of the lenght of a single straight to the ring circumference is .43. There will be a near detector hall located approximately 50 m from the end of the straight (as shown in Fig. 23) and nuSTORM will use the existing D0 assembly building (DAB) as the far (1.5 km) detector hall. The pit area of DAB can accommodate a 1-1.5 kT of magnetized iron detector plus a LAr detector in the range of 500 - 1000T.

It is expected that all civil construction at the Fermilab site will be at the Main Injector depth of 21 feet below grade although some additional over burden may be required for the target hall. An engineering concept

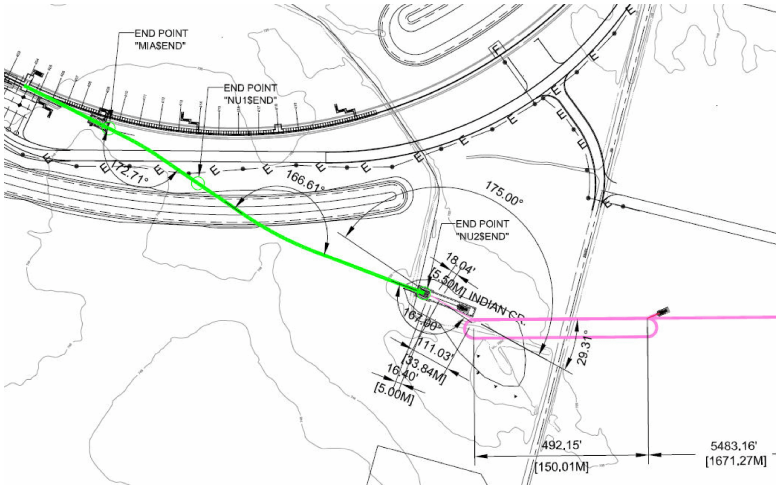

Figure 24: Schematic of site detail

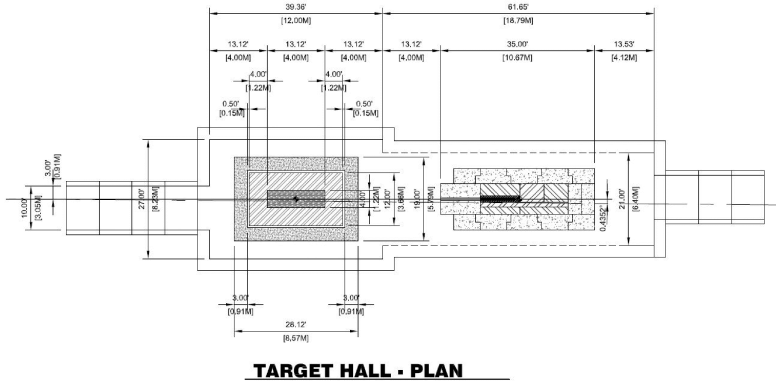

Figure 25: Schematic of the target hall

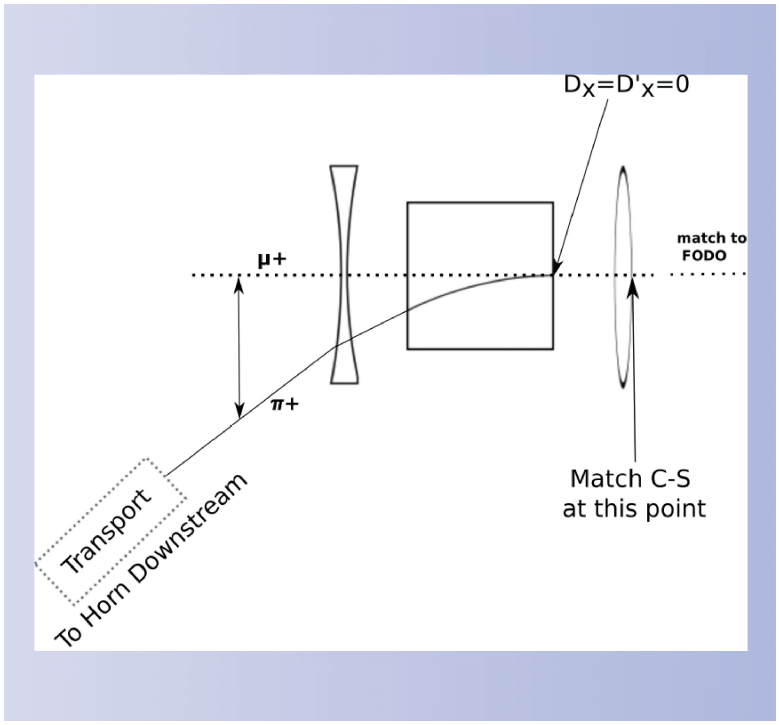

Figure 26: Stochastic Injection section

fo the underground tunneling is shown in Fig. 27. The site location described above is ideal for nuSTORM. The needed services (water and power) are nearby, but the area is essentially open and underveloped so that nuSTORM construction will not interfer (or have to accommodate) existing infrastructure. In addition, being able to use the D0 Assembly Building as the far detector hall represents a significant cost savings.

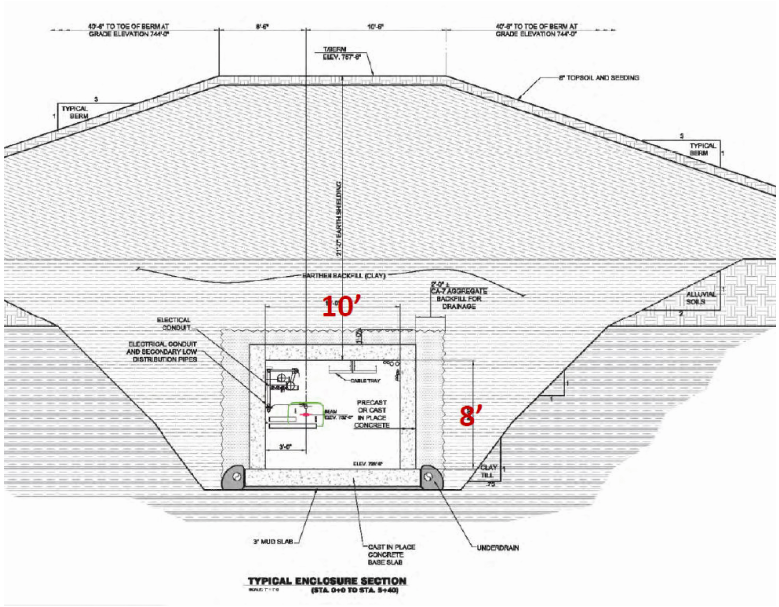

Figure 27: Schematic of tunneling

5 Proposed programme

Lead authors: Long, Wildner
Page limit: 4

6 Summary

Lead authors: Long, Bross
Page limit: 1

References

[1] B. Pontecorvo, "Mesonium and antimesonium," *Sov. Phys. JETP* **6** (1957) 429.

[2] B. Pontecorvo, "Inverse beta processes and nonconservation of lepton charge," *Sov. Phys. JETP* **7** (1958) 172–173.

[3] Z. Maki, M. Nakagawa, and S. Sakata, "Remarks on the unified model of elementary particles," *Prog. Theor. Phys.* **28** (1962) 870–880.

[4] S. M. Bilenky, S. Pascoli, and S. T. Petcov, "Majorana neutrinos, neutrino mass spectrum, CP-violation and neutrinoless double beta-decay. I: The three-neutrino mixing case," *Phys. Rev. D* **64** (2001) 053010, arXiv:0102265 [hep-ph].

[5] C. Amsler *et al.*, "Review of particle physics," *Physics Letters B* **667** no. 1-5, (2008) 1–6. http://pdg.lbl.gov. and 2009 partial update for 2010 edition.

[6] **LSND** Collaboration, A. Aguilar *et al.*, "Evidence for neutrino oscillations from the observation of $\bar{\nu}_e$ appearance in a $\bar{\nu}_\mu$ beam," *Phys. Rev. D* **64** (2001) 112007, arXiv:0104049 [hep-ex].

[7] **MiniBooNE** Collaboration, A. A. Aguilar-Arevalo *et al.*, "A search for electron neutrino appearance at the $\Delta m^2 \sim 1$ eV^2 scale," *Phys. Rev. Lett.* **98** (2007) 231801, arXiv:0704.1500 [hep-ex].

[8] **MiniBooNE Collaboration** Collaboration, A. Aguilar-Arevalo *et al.*, "Event Excess in the MiniBooNE Search for $\bar{\nu}_\mu \to \bar{\nu}_e$ Oscillations," *Phys.Rev.Lett.* **105** (2010) 181801, arXiv:1007.1150 [hep-ex].

[9] T. Mueller, D. Lhuillier, M. Fallot, A. Letourneau, S. Cormon, *et al.*, "Improved Predictions of Reactor Antineutrino Spectra," *Phys.Rev.* **C83** (2011) 054615, arXiv:1101.2663 [hep-ex].

[10] P. Huber, "Determination of anti-neutrino spectra from nuclear reactors," *Phys.Rev.* **C84** (2011) 024617, arXiv:1106.0687 [hep-ph].

[11] G. Mention, M. Fechner, T. Lasserre, T. Mueller, D. Lhuillier, *et al.*, "The Reactor Antineutrino Anomaly," *Phys.Rev.* **D83** (2011) 073006, arXiv:1101.2755 [hep-ex].

[12] **GALLEX Collaboration.** Collaboration, P. Anselmann *et al.*, "First results from the Cr-51 neutrino source experiment with the GALLEX detector," *Phys.Lett.* **B342** (1995) 440–450.

[13] **GALLEX Collaboration** Collaboration, W. Hampel *et al.*, "Final results of the Cr-51 neutrino source experiments in GALLEX," *Phys.Lett.* **B420** (1998) 114–126.

[14] J. Abdurashitov, V. Gavrin, S. Girin, V. Gorbachev, T. V. Ibragimova, *et al.*, "The Russian-American gallium experiment (SAGE) Cr neutrino source measurement," *Phys.Rev.Lett.* **77** (1996) 4708–4711.

[15] **SAGE Collaboration** Collaboration, J. Abdurashitov *et al.*, "Measurement of the response of the Russian-American gallium experiment to neutrinos from a Cr-51 source," *Phys.Rev.* **C59** (1999) 2246–2263, arXiv:hep-ph/9803418 [hep-ph].

[16] **SAGE Collaboration** Collaboration, J. Abdurashitov, V. Gavrin, S. Girin, V. Gorbachev, P. Gurkina, *et al.*, "Measurement of the response of a Ga solar neutrino experiment to neutrinos from an Ar-37 source," *Phys.Rev.* **C73** (2006) 045805, arXiv:nucl-ex/0512041 [nucl-ex].

[17] K. Abazajian, M. Acero, S. Agarwalla, A. Aguilar-Arevalo, C. Albright, *et al.*, "Light Sterile Neutrinos: A White Paper," arXiv:1204.5379 [hep-ph].

[18] **nuSTORM Collaboration** Collaboration, P. Kyberd *et al.*, "nuSTORM - Neutrinos from STORed Muons: Letter of Intent to the Fermilab Physics Advisory Committee," arXiv:1206.0294 [hep-ex].

[19] **DAYA-BAY Collaboration** Collaboration, F. An *et al.*, "Observation of electron-antineutrino disappearance at Daya Bay," *Phys.Rev.Lett.* **108** (2012) 171803, arXiv:1203.1669 [hep-ex].

[20] **RENO collaboration** Collaboration, J. Ahn *et al.*, "Observation of Reactor Electron Antineutrino Disappearance in the RENO Experiment," *Phys.Rev.Lett.* **108** (2012) 191802, arXiv:1204.0626 [hep-ex].

[21] **DOUBLE-CHOOZ Collaboration** Collaboration, Y. Abe *et al.*, "Indication for the reactor anti-neutrino disappearance in the Double Chooz experiment," *Phys.Rev.Lett.* **108** (2012) 131801, arXiv:1112.6353 [hep-ex].

[22] **T2K Collaboration** Collaboration, K. Abe *et al.*, "Indication of Electron Neutrino Appearance from an Accelerator-produced Off-axis Muon Neutrino Beam," *Phys.Rev.Lett.* **107** (2011) 041801, arXiv:1106.2822 [hep-ex].

[23] **MINOS Collaboration** Collaboration, P. Adamson *et al.*, "Improved search for muon-neutrino to electron-neutrino oscillations in MINOS," *Phys.Rev.Lett.* **107** (2011) 181802, arXiv:1108.0015 [hep-ex].

[24] P. Huber, M. Mezzetto, and T. Schwetz, "On the impact of systematical uncertainties for the CP violation measurement in superbeam experiments," *JHEP* **03** (2008) 021, arXiv:0711.2950 [hep-ph].

[25] P. Coloma, P. Huber, J. Kopp, and W. Winter, "Systematic uncertainties in long-baseline neutrino oscillations for large θ_{13}," arXiv:1209.5973 [hep-ph].

[26] t. . Harvard Universitry"=.

[27] **IDS-NF Collaboration** Collaboration, S. Choubey *et al.*, "International Design Study for the Neutrino Factory, Interim Design Report," arXiv:1112.2853 [hep-ex].

[28] S. D. Holmes and V. D. Shiltsev, "Muon Collider," arXiv:1202.3803 [physics.acc-ph].

[29] M. Bando and K. Yoshioka, "Sterile neutrinos in a grand unified model," *Prog.Theor.Phys.* **100** (1998) 1239–1250, arXiv:hep-ph/9806400 [hep-ph].

[30] E. Ma, "Neutrino masses in an extended gauge model with E(6) particle content," *Phys.Lett.* **B380** (1996) 286–290, arXiv:hep-ph/9507348 [hep-ph].

[31] Q. Shafi and Z. Tavartkiladze, "Neutrino mixings and fermion masses in supersymmetric SU(5)," *Phys.Lett.* **B451** (1999) 129–135, arXiv:hep-ph/9901243 [hep-ph].

[32] K. Babu and G. Seidl, "Chiral gauge models for light sterile neutrinos," *Phys.Rev.* **D70** (2004) 113014, arXiv:hep-ph/0405197 [hep-ph].

[33] A. Kusenko, F. Takahashi, and T. T. Yanagida, "Dark Matter from Split Seesaw," *Phys.Lett.* **B693** (2010) 144–148, arXiv:1006.1731 [hep-ph].

[34] R. Mohapatra, "Connecting bimaximal neutrino mixing to a light sterile neutrino," *Phys.Rev.* **D64** (2001) 091301, arXiv:hep-ph/0107264 [hep-ph].

[35] C. D. Froggatt and H. B. Nielsen, "Hierarchy of quark masses, cabibbo angles and cp violation," *Nucl. Phys.* **B147** (1979) 277.

[36] J. Barry, W. Rodejohann, and H. Zhang, "Sterile Neutrinos for Warm Dark Matter and the Reactor Anomaly in Flavor Symmetry Models," *JCAP* **1201** (2012) 052, arXiv:1110.6382 [hep-ph].

[37] R. Mohapatra, S. Nasri, and H.-B. Yu, "Seesaw right handed neutrino as the sterile neutrino for LSND," *Phys.Rev.* **D72** (2005) 033007, arXiv:hep-ph/0505021 [hep-ph].

[38] C. S. Fong, R. N. Mohapatra, and I. Sung, "Majorana Neutrinos from Inverse Seesaw in Warped Extra Dimension," *Phys.Lett.* **B704** (2011) 171–178, arXiv:1107.4086 [hep-ph].

[39] H. Zhang, "Light Sterile Neutrino in the Minimal Extended Seesaw," *Phys.Lett.* **B714** (2012) 262–266, arXiv:1110.6838 [hep-ph].

[40] Z. G. Berezhiani and R. N. Mohapatra, "Reconciling present neutrino puzzles: Sterile neutrinos as mirror neutrinos," *Phys. Rev.* **D52** (1995) 6607–6611, hep-ph/9505385.

[41] R. Foot and R. R. Volkas, "Neutrino physics and the mirror world: How exact parity symmetry explains the solar neutrino deficit, the atmospheric neutrino anomaly and the lsnd experiment," *Phys. Rev.* **D52** (1995) 6595–6606, hep-ph/9505359.

[42] V. Berezinsky, M. Narayan, and F. Vissani, "Mirror model for sterile neutrinos," *Nucl.Phys.* **B658** (2003) 254–280, arXiv:hep-ph/0210204 [hep-ph].

[43] **MiniBooNE Collaboration** Collaboration, A. Aguilar-Arevalo *et al.*, "A Combined $\nu_\mu \to \nu_e$ and $\bar{\nu}_\mu \to \bar{\nu}_e$ Oscillation Analysis of the MiniBooNE Excesses," arXiv:1207.4809 [hep-ex].

[44] K. Schreckenbach, G. Colvin, W. Gelletly, and F. Von Feilitzsch, "DETERMINATION OF THE ANTI-NEUTRINO SPECTRUM FROM U-235 THERMAL NEUTRON FISSION PRODUCTS UP TO 9.5-MEV," *Phys.Lett.* **B160** (1985) 325–330.

[45] M. A. Acero, C. Giunti, and M. Laveder, "Limits on nu(e) and anti-nu(e) disappearance from Gallium and reactor experiments," *Phys.Rev.* **D78** (2008) 073009, arXiv:0711.4222 [hep-ph].

[46] C. Giunti and M. Laveder, "Short-Baseline Electron Neutrino Disappearance, Tritium Beta Decay and Neutrinoless Double-Beta Decay," arXiv:1005.4599 [hep-ph].

[47] C. Giunti and M. Laveder, "Statistical Significance of the Gallium Anomaly," *Phys.Rev.* **C83** (2011) 065504, arXiv:1006.3244 [hep-ph].

[48] **KARMEN** Collaboration, B. Armbruster *et al.*, "Upper limits for neutrino oscillations anti-nu/mu $\to$ anti- nu/e from muon decay at rest," *Phys. Rev.* **D65** (2002) 112001, hep-ex/0203021.

[49] **NOMAD** Collaboration, P. Astier *et al.*, "Final NOMAD results on nu/mu –¿ nu/tau and nu/e –¿ nu/tau oscillations including a new search for nu/tau appearance using hadronic tau decays," *Nucl. Phys.* **B611** (2001) 3–39, arXiv:hep-ex/0106102.

[50] L. Borodovsky, C. Chi, Y. Ho, N. Kondakis, W.-Y. Lee, *et al.*, "Search for muon-neutrino oscillations $\nu_\mu \to \nu_e$ ($\bar{\nu}_\mu \to \bar{\nu}_e$) in a wide band neutrino beam," *Phys.Rev.Lett.* **68** (1992) 274–277.

[51] M. Antonello, B. Baibussinov, P. Benetti, E. Calligarich, N. Canci, *et al.*, "Experimental search for the LSND anomaly with the ICARUS LAr TPC detector in the CNGS beam," arXiv:1209.0122 [hep-ex].

[52] **Super-Kamiokande** Collaboration, Y. Ashie *et al.*, "A measurement of atmospheric neutrino oscillation parameters by super-kamiokande i," *Phys. Rev.* **D71** (2005) 112005, hep-ex/0501064.

[53] B. T. Cleveland *et al.*, "Measurement of the solar electron neutrino flux with the Homestake chlorine detector," *Astrophys. J.* **496** (1998) 505–526.

[54] F. Kaether, W. Hampel, G. Heusser, J. Kiko, and T. Kirsten, "Reanalysis of the GALLEX solar neutrino flux and source experiments," *Phys. Lett. B* **685** (2010) 47–54, arXiv:1001.2731 [hep-ex].

[55] **SAGE** Collaboration, J. N. Abdurashitov *et al.*, "Measurement of the solar neutrino capture rate with gallium metal. III: Results for the 2002–2007 data-taking period," *Phys. Rev. C* **80** (2009) 015807, arXiv:0901.2200 [nucl-ex].

[56] **Super-Kamkiokande** Collaboration, J. Hosaka *et al.*, "Solar neutrino measurements in Super-Kamiokande-I," *Phys. Rev. D* **73** (2006) 112001, arXiv:0508053 [hep-ex].

[57] **SNO** Collaboration, B. Aharmim *et al.*, "Measurement of the ν_e and total B-8 solar neutrino fluxes with the Sudbury Neutrino Observatory phase I data set," *Phys. Rev.* **C75** (2007) 045502, arXiv:nucl-ex/0610020.

[58] **SNO** Collaboration, B. Aharmim *et al.*, "Electron energy spectra, fluxes, and day-night asymmetries of b-8 solar neutrinos from the 391-day salt phase sno data set," *Phys. Rev.* **C72** (2005) 055502, nucl-ex/0502021.

[59] **SNO** Collaboration, B. Aharmim *et al.*, "An Independent Measurement of the Total Active ^{8}B Solar Neutrino Flux Using an Array of ^{3}He Proportional Counters at the Sudbury Neutrino Observatory," *Phys. Rev. Lett.* **101** (2008) 111301, arXiv:0806.0989 [nucl-ex].

[60] **SNO** Collaboration, B. Aharmim *et al.*, "Combined Analysis of all Three Phases of Solar Neutrino Data from the Sudbury Neutrino Observatory," arXiv:1109.0763 [nucl-ex].

[61] **Borexino** Collaboration, G. Bellini *et al.*, "Precision measurement of the 7Be solar neutrino interaction rate in Borexino," *Phys.Rev.Lett.* **107** (2011) 141302, arXiv:1104.1816 [hep-ex].

[62] **Borexino Collaboration** Collaboration, G. Bellini *et al.*, "Measurement of the solar 8B neutrino rate with a liquid scintillator target and 3 MeV energy threshold in the Borexino detector," *Phys.Rev.* **D82** (2010) 033006, arXiv:0808.2868 [astro-ph].

[63] **MINOS** Collaboration, P. Adamson *et al.*, "Search for sterile neutrino mixing in the MINOS long-baseline experiment," (2010) , arXiv:1001.0336 [hep-ex].

[64] **MINOS Collaboration** Collaboration, P. Adamson *et al.*, "Active to sterile neutrino mixing limits from neutral-current interactions in MINOS," *Phys.Rev.Lett.* (2011) , arXiv:1104.3922 [hep-ex].

[65] F. Dydak *et al.*, "A Search for Muon-neutrino Oscillations in the Δm^2 Range 0.3-eV^2 to 90-eV^2," *Phys. Lett. B* **134** (1984) 281.

[66] J. Kopp, M. Maltoni, and T. Schwetz, "Are there sterile neutrinos at the eV scale?," *Phys.Rev.Lett.* **107** (2011) 091801, arXiv:1103.4570 [hep-ph].

[67] C. Giunti and M. Laveder, "Implications of 3+1 Short-Baseline Neutrino Oscillations," *Phys.Lett.* **B706** (2011) 200–207, arXiv:1111.1069 [hep-ph].

[68] G. Karagiorgi, "Confronting Recent Neutrino Oscillation Data with Sterile Neutrinos," arXiv:1110.3735 [hep-ph].

[69] C. Giunti and M. Laveder, "Status of 3+1 Neutrino Mixing," *Phys.Rev.* **D84** (2011) 093006, arXiv:1109.4033 [hep-ph].

[70] C. Giunti and M. Laveder, "3+1 and 3+2 Sterile Neutrino Fits," *Phys.Rev.* **D84** (2011) 073008, arXiv:1107.1452 [hep-ph].

[71] J. Kopp, P. Machado, M. Maltoni, and T. Schwetz. Work in progress.

[72] **MiniBooNE** Collaboration, A. A. Aguilar-Arevalo *et al.*, "A search for muon neutrino and antineutrino disappearance in MiniBooNE," *Phys. Rev. Lett.* **103** (2009) 061802, arXiv:0903.2465 [hep-ex].

[73] **MiniBooNE Collaboration, SciBooNE Collaboration** Collaboration, G. Cheng *et al.*, "Dual baseline search for muon antineutrino disappearance at $0.1\text{eV}^2 < \Delta m^2 < 100\text{eV}^2$," arXiv:1208.0322 [hep-ex]. Data and analysis instructions available at http://www-sciboone.fnal.gov/data_release/joint_numubar_disap/.

[74] Y. Declais *et al.*, "Search for neutrino oscillations at 15-meters, 40-meters, and 95-meters from a nuclear power reactor at bugey," *Nucl. Phys. B* **434** (1995) 503–534.

[75] Y. Declais, H. de Kerret, B. Lefievre, M. Obolensky, A. Etenko, *et al.*, "Study of reactor anti-neutrino interaction with proton at Bugey nuclear power plant," *Phys.Lett.* **B338** (1994) 383–389.

[76] A. Kuvshinnikov, L. Mikaelyan, S. Nikolaev, M. Skorokhvatov, and A. Etenko, "Measuring the anti-electron-neutrino + p -¿ n + e+ cross-section and beta decay axial constant in a new experiment at Rovno NPP reactor. (In Russian)," *JETP Lett.* **54** (1991) 253–257.

[77] G. Vidyakin, V. Vyrodov, I. Gurevich, Y. Kozlov, V. Martemyanov, *et al.*, "DETECTION OF ANTI-NEUTRINOS IN THE FLUX FROM TWO REACTORS," *Sov.Phys.JETP* **66** (1987) 243–247.

[78] H. Kwon, F. Boehm, A. Hahn, H. Henrikson, J. Vuilleumier, *et al.*, "Search for neutrino oscillations at a fission reactor," *Phys.Rev.* **D24** (1981) 1097–1111.

[79] **CALTECH-SIN-TUM** Collaboration, G. Zacek *et al.*, "Neutrino oscillation experiments at the gosgen nuclear power reactor," *Phys. Rev.* **D34** (1986) 2621–2636.

[80] **CHOOZ** Collaboration, M. Apollonio *et al.*, "Search for neutrino oscillations on a long base-line at the CHOOZ nuclear power station," *Eur. Phys. J. C* **27** (2003) 331–374, arXiv:0301017 [hep-ex].

[81] F. Boehm *et al.*, "Final results from the palo verde neutrino oscillation experiment," *Phys. Rev.* **D64** (2001) 112001, hep-ex/0107009.

[82] D. Dwyer, "Daya Bay results." Talk at Neutrino2012, 3–9 June 2012, Kyoto, Japan, 2012.

[83] **Double Chooz Collaboration** Collaboration, Y. Abe *et al.*, "Reactor electron antineutrino disappearance in the Double Chooz experiment," *Phys.Rev.* **D86** (2012) 052008, arXiv:1207.6632 [hep-ex].

[84] **KamLAND** Collaboration, A. Gando *et al.*, "Constraints on θ_{13} from A Three-Flavor Oscillation Analysis of Reactor Antineutrinos at KamLAND," arXiv:1009.4771 [hep-ex].

[85] J. Reichenbacher, "Final KARMEN results on neutrino oscillations and neutrino nucleus interactions in the energy regime of supernovae,". PhD thesis, Univ. Karlsruhe.

[86] **LSND Collaboration** Collaboration, L. Auerbach *et al.*, "Measurements of charged current reactions of nu(e) on 12-C," *Phys.Rev.* **C64** (2001) 065501, arXiv:hep-ex/0105068 [hep-ex].

[87] P. Huber, M. Lindner, and W. Winter, "Simulation of long-baseline neutrino oscillation experiments with GLoBES," *Comput. Phys. Commun.* **167** (2005) 195, hep-ph/0407333. http://www.mpi-hd.mpg.de/~globes.

[88] P. Huber, J. Kopp, M. Lindner, M. Rolinec, and W. Winter, "New features in the simulation of neutrino oscillation experiments with GLoBES 3.0," *Comput. Phys. Commun.* **177** (2007) 432–438, hep-ph/0701187. http://www.mpi-hd.mpg.de/~globes.

[89] M. C. Gonzalez-Garcia and M. Maltoni, "Phenomenology with Massive Neutrinos," *Phys. Rept.* **460** (2008) 1–129, arXiv:0704.1800 [hep-ph].

[90] M. Maltoni and T. Schwetz, "Sterile neutrino oscillations after first MiniBooNE results," *Phys. Rev. D* **76** (2007) 093005, arXiv:0705.0107 [hep-ph].

[91] E. Akhmedov and T. Schwetz, "MiniBooNE and LSND data: non-standard neutrino interactions in a (3+1) scheme versus (3+2) oscillations," arXiv:1007.4171 [hep-ph].

[92] M. Maltoni and T. Schwetz, "Testing the statistical compatibility of independent data sets," *Phys. Rev. D* **68** (2003) 033020, arXiv:0304176 [hep-ph].

[93] S. Joudaki, K. N. Abazajian, and M. Kaplinghat, "Are Light Sterile Neutrinos Preferred or Disfavored by Cosmology?," arXiv:1208.4354 [astro-ph.CO].

[94] M. Gonzalez-Garcia, M. Maltoni, and J. Salvado, "Robust Cosmological Bounds on Neutrinos and their Combination with Oscillation Results," *JHEP* **1008** (2010) 117, arXiv:1006.3795 [hep-ph].

[95] J. Hamann, S. Hannestad, G. G. Raffelt, I. Tamborra, and Y. Y. Y. Wong, "Cosmology seeking friendship with sterile neutrinos," arXiv:1006.5276 [hep-ph].

[96] E. Giusarma, M. Corsi, M. Archidiacono, R. de Putter, A. Melchiorri, *et al.*, "Constraints on massive sterile neutrino species from current and future cosmological data," *Phys.Rev.* **D83** (2011) 115023, arXiv:1102.4774 [astro-ph.CO].

[97] G. Mangano and P. D. Serpico, "A robust upper limit on $N_{\rm eff}$ from BBN, circa 2011," *Phys.Lett.* **B701** (2011) 296–299, arXiv:1103.1261 [astro-ph.CO].

[98] J. Hamann, S. Hannestad, G. G. Raffelt, and Y. Y. Wong, "Sterile neutrinos with eV masses in cosmology: How disfavoured exactly?," *JCAP* **1109** (2011) 034, arXiv:1108.4136 [astro-ph.CO].

[99] L. Bento and Z. Berezhiani, "Blocking active sterile neutrino oscillations in the early universe with a Majoron field," *Phys.Rev.* **D64** (2001) 115015, arXiv:hep-ph/0108064 [hep-ph].

[100] A. Dolgov and F. Takahashi, "Do neutrino flavor oscillations forbid large lepton asymmetry of the universe?," *Nucl.Phys.* **B688** (2004) 189–213, arXiv:hep-ph/0402066 [hep-ph].

[101] G. Karagiorgi, M. Shaevitz, and J. Conrad, "Confronting the short-baseline oscillation anomalies with a single sterile neutrino and non-standard matter effects," arXiv:1202.1024 [hep-ph].

[102] **Particle Data Group** Collaboration, J. Beringer *et al.*, "Review of Particle Physics (RPP)," *Phys.Rev.* **D86** (2012) 010001.

[103] **LBNE Collaboration** Collaboration, T. Akiri *et al.*, "The 2010 Interim Report of the Long-Baseline Neutrino Experiment Collaboration Physics Working Groups," arXiv:1110.6249 [hep-ex].

[104] A. Rubbia *et al.*, "Expression of Interest for a very long baseline neutrino oscillation experiment (LBNO)." Https://cdsweb.cern.ch/record/1457543/files/spsc-eoi-007.pd, 2012.

[105] K. Abe, T. Abe, H. Aihara, Y. Fukuda, Y. Hayato, *et al.*, "Letter of Intent: The Hyper-Kamiokande Experiment — Detector Design and Physics Potential —," arXiv:1109.3262 [hep-ex].

[106] C. Llewellyn Smith, "Neutrino Reactions at Accelerator Energies," *Phys.Rept.* **3** (1972) 261–379.

[107] R. Smith and E. Moniz, "NEUTRINO REACTIONS ON NUCLEAR TARGETS," *Nucl.Phys.* **B43** (1972) 605.

[108] D. Rein and L. M. Sehgal, "Neutrino Excitation of Baryon Resonances and Single Pion Production," *Annals Phys.* **133** (1981) 79–153.

[109] **K2K Collaboration** Collaboration, R. Gran *et al.*, "Measurement of the quasi-elastic axial vector mass in neutrino-oxygen interactions," *Phys.Rev.* **D74** (2006) 052002, arXiv:hep-ex/0603034 [hep-ex].

[110] **K2K Collaboration** Collaboration, A. Rodriguez *et al.*, "Measurement of single charged pion production in the charged-current interactions of neutrinos in a 1.3-GeV wide band beam," *Phys.Rev.* **D78** (2008) 032003, arXiv:0805.0186 [hep-ex].

[111] **K2K Collaboration** Collaboration, C. Mariani, "Charged current neutral pion cross section measurement at K2K," *AIP Conf.Proc.* **1189** (2009) 339–342.

[112] **K2K Collaboration** Collaboration, S. Nakayama *et al.*, "Measurement of single pi0 production in neutral current neutrino interactions with water by a 1.3-GeV wide band muon neutrino beam," *Phys.Lett.* **B619** (2005) 255–262, arXiv:hep-ex/0408134 [hep-ex].

[113] **MiniBooNE Collaboration** Collaboration, A. Aguilar-Arevalo *et al.*, "Measurement of muon neutrino quasi-elastic scattering on carbon," *Phys.Rev.Lett.* **100** (2008) 032301, arXiv:0706.0926 [hep-ex].

[114] **MiniBooNE Collaboration** Collaboration, A. Aguilar-Arevalo *et al.*, "First Measurement of the Muon Neutrino Charged Current Quasielastic Double Differential Cross Section," *Phys.Rev.* **D81** (2010) 092005, arXiv:1002.2680 [hep-ex].

[115] **MiniBooNE Collaboration** Collaboration, A. Aguilar-Arevalo *et al.*, "Measurement of the ν_μ charged current π^+ to quasi-elastic cross section ratio on mineral oil in a 0.8-GeV neutrino beam," *Phys.Rev.Lett.* **103** (2009) 081801, arXiv:0904.3159 [hep-ex].

[116] **MiniBooNE Collaboration** Collaboration, A. Aguilar-Arevalo *et al.*, "Measurement of Neutrino-Induced Charged-Current Charged Pion Production Cross Sections on Mineral Oil at $E_\nu \sim 1$ GeV," *Phys.Rev.* **D83** (2011) 052007, arXiv:1011.3572 [hep-ex].

[117] **MiniBooNE Collaboration** Collaboration, A. Aguilar-Arevalo *et al.*, "Measurement of ν_μ-induced charged-current neutral pion production cross sections on mineral oil at $E_\nu \in 0.5 - 2.0$ GeV," *Phys.Rev.* **D83** (2011) 052009, arXiv:1010.3264 [hep-ex].

[118] **MiniBooNE Collaboration** Collaboration, A. A. Aguilar-Arevalo *et al.*, "Measurement of nu(mu) and anti-nu(mu) induced neutral current single pi0 production cross sections on mineral oil at E(nu) O(1-GeV)," *Phys.Rev.* **D81** (2010) 013005, arXiv:0911.2063 [hep-ex].

[119] **MiniBooNE Collaboration** Collaboration, A. Aguilar-Arevalo *et al.*, "Measurement of the Neutrino Neutral-Current Elastic Differential Cross Section on Mineral Oil at $E_\nu \sim 1$ GeV," *Phys.Rev.* **D82** (2010) 092005, arXiv:1007.4730 [hep-ex].

[120] **SciBooNE Collaboration** Collaboration, J. L. Alcaraz-Aunion and J. Walding, "Measurement of the nu(mu)-CCQE cross-section in the SciBooNE experiment," *AIP Conf.Proc.* **1189** (2009) 145–150, arXiv:0909.5647 [hep-ex].

[121] **SciBooNE Collaboration** Collaboration, Y. Nakajima *et al.*, "Measurement of inclusive charged current interactions on carbon in a few-GeV neutrino beam," *Phys.Rev.* **D83** (2011) 012005, arXiv:1011.2131 [hep-ex].

[122] **SciBooNE Collaboration** Collaboration, Y. Kurimoto *et al.*, "Measurement of Inclusive Neutral Current Neutral pi0 Production on Carbon in a Few-GeV Neutrino Beam," *Phys.Rev.* **D81** (2010) 033004, arXiv:0910.5768 [hep-ex].

[123] **SciBooNE Collaboration** Collaboration, Y. Kurimoto *et al.*, "Improved measurement of neutral current coherent π^0 production on carbon in a few-GeV neutrino beam," *Phys.Rev.* **D81** (2010) 111102, arXiv:1005.0059 [hep-ex].

[124] H. Gallagher, G. Garvey, and G. Zeller, "Neutrino-nucleus interactions," *Ann.Rev.Nucl.Part.Sci.* **61** (2011) 355–378.

[125] J. G. Morfin, J. Nieves, and J. T. Sobczyk, "Recent Developments in Neutrino/Antineutrino - Nucleus Interactions," arXiv:1209.6586 [hep-ex].

[126] A. M. Ankowski, "Breakdown of the impulse approximation and its consequences: The Low-Q**2 problem," *PoS* **NUFACT08** (2008) 118, arXiv:0810.1167 [nucl-th].

[127] O. Benhar, N. Farina, H. Nakamura, M. Sakuda, and R. Seki, "Lepton-nucleus scattering in the impulse approximation regime," *Nucl.Phys.Proc.Suppl.* **155** (2006) 254–256, arXiv:hep-ph/0510259 [hep-ph].

[128] M. Martini, M. Ericson, G. Chanfray, and J. Marteau, "A Unified approach for nucleon knock-out, coherent and incoherent pion production in neutrino interactions with nuclei," *Phys.Rev.* **C80** (2009) 065501, arXiv:0910.2622 [nucl-th].

[129] J. Nieves, I. Ruiz Simo, and M. Vicente Vacas, "Inclusive Charged–Current Neutrino–Nucleus Reactions," *Phys.Rev.* **C83** (2011) 045501, arXiv:1102.2777 [hep-ph].

[130] A. Bodek, S. Avvakumov, R. Bradford, and H. S. Budd, "Vector and Axial Nucleon Form Factors:A Duality Constrained Parameterization," *Eur.Phys.J.* **C53** (2008) 349–354, arXiv:0708.1946 [hep-ex].

[131] V. Bernard, L. Elouadrhiri, and U.-G. Meissner, "Axial structure of the nucleon," *Journal of Physics G: Nuclear and Particle Physics* **28** no. 1, (2002) R1. http://stacks.iop.org/0954-3899/28/i=1/a=201.

[132] J. Nieves, I. Ruiz Simo, and M. Vicente Vacas, "The nucleon axial mass and the MiniBooNE Quasielastic Neutrino-Nucleus Scattering problem," *Phys.Lett.* **B707** (2012) 72–75, arXiv:1106.5374 [hep-ph].

[133] M. Martini, M. Ericson, and G. Chanfray, "Neutrino quasielastic interaction and nuclear dynamics," *Phys.Rev.* **C84** (2011) 055502, arXiv:1110.0221 [nucl-th].

[134] A. Meucci and C. Giusti, "Relativistic descriptions of final-state interactions in charged-current quasielastic antineutrino-nucleus scattering at MiniBooNE kinematics," *Phys.Rev.* **D85** (2012) 093002, arXiv:1202.4312 [nucl-th].

[135] J. Amaro, M. Barbaro, J. Caballero, T. Donnelly, and J. Udias, "Relativistic analyses of quasielastic neutrino cross sections at MiniBooNE kinematics," *Phys.Rev.* **D84** (2011) 033004, arXiv:1104.5446 [nucl-th].

[136] A. Bodek, H. Budd, and M. Christy, "Neutrino Quasielastic Scattering on Nuclear Targets: Parametrizing Transverse Enhancement (Meson Exchange Currents)," *Eur.Phys.J.* **C71** (2011) 1726, arXiv:1106.0340 [hep-ph].

[137] J. T. Sobczyk, "Transverse Enhancement Model and MiniBooNE Charge Current Quasi-Elastic Neutrino Scattering Data," *Eur.Phys.J.* **C72** (2012) 1850, arXiv:1109.1081 [hep-ex].

[138] O. Lalakulich and U. Mosel, "Energy reconstruction in quasielastic scattering in the MiniBooNE and T2K experiments," *Phys.Rev.* **C86** (2012) 054606, arXiv:1208.3678 [nucl-th].

[139] O. Lalakulich, K. Gallmeister, and U. Mosel, "Neutrino- and antineutrino-induced reactions with nuclei between 1 and 50 GeV," *Phys.Rev.* **C86** (2012) 014607, arXiv:1205.1061 [nucl-th].

[140] M. Martini, M. Ericson, and G. Chanfray, "Neutrino energy reconstruction problems and neutrino oscillations," *Phys.Rev.* **D85** (2012) 093012, arXiv:1202.4745 [hep-ph].

[141] J. T. Sobczyk, "Multinucleon Ejection Model for Two Body Current Neutrino Interactions,".

[142] J. A. Formaggio and G. P. Zeller, "From ev to eev: Neutrino cross sections across energy scales," *Rev. Mod. Phys.* **84** (Sep, 2012) 1307–1341. http://link.aps.org/doi/10.1103/RevModPhys.84.1307.

[143] **Gargamelle Neutrino Propane Collaboration, Aachen-Brussels-CERN-Ecole Poly-Orsay-Padua Collaboration** Collaboration, W. Krenz *et al.*, "Experimental Study of Exclusive One Pion Production in All Neutrino Induced Neutral Current Channels," *Nucl.Phys.* **B135** (1978) 45–65.

[144] O. Lalakulich, K. Gallmeister, T. Leitner, and U. Mosel, "Pion production in the MiniBooNE," *AIP Conf.Proc.* **1405** (2011) 127–133, arXiv:1107.5947 [nucl-th].

[145] **K2K Collaboration** Collaboration, C. Mariani *et al.*, "Measurement of inclusive π^0 production in the Charged-Current Interactions of Neutrinos in a 1.3-GeV wide band beam," *Phys.Rev.* **D83** (2011) 054023, arXiv:1012.1794 [hep-ex].

[146] **K2K Collaboration** Collaboration, H. Tanaka, "K2K coherent pion production in SciBar," *Nucl.Phys.Proc.Suppl.* **159** (2006) 38–43.

[147] **NOMAD Collaboration** Collaboration, C. Kullenberg *et al.*, "A Measurement of Coherent Neutral Pion Production in Neutrino Neutral Current Interactions in NOMAD," *Phys.Lett.* **B682** (2009) 177–184, arXiv:0910.0062 [hep-ex].

[148] D. Rein and L. Sehgal, "COHERENT PRODUCTION OF PHOTONS BY NEUTRINOS," *Phys.Lett.* **B104** (1981) 394–398.

[149] **MiniBooNE Collaboration** Collaboration, A. Aguilar-Arevalo *et al.*, "First Observation of Coherent π^0 Production in Neutrino Nucleus Interactions with $E_\nu < 2$ GeV," *Phys.Lett.* **B664** (2008) 41–46, arXiv:0803.3423 [hep-ex].

[150] **K2K Collaboration** Collaboration, M. Hasegawa *et al.*, "Search for coherent charged pion production in neutrino-carbon interactions," *Phys.Rev.Lett.* **95** (2005) 252301, arXiv:hep-ex/0506008 [hep-ex].

[151] **SciBooNE Collaboration** Collaboration, K. Hiraide, "Search for neutrino charged current coherent pion production in SciBooNE," *Nuovo Cim.* **C32N5-6** (2009) 75–82.

[152] J. Amaro, E. Hernandez, J. Nieves, and M. Valverde, "Theoretical study of neutrino-induced coherent pion production off nuclei at T2K and MiniBooNE energies," *Phys.Rev.* **D79** (2009) 013002, arXiv:0811.1421 [hep-ph].

[153] S. Nakamura, T. Sato, T.-S. Lee, B. Szczerbinska, and K. Kubodera, "Dynamical Model of Coherent Pion Production in Neutrino-Nucleus Scattering," *Phys.Rev.* **C81** (2010) 035502, arXiv:0910.1057 [nucl-th].

[154] **T2K Collaboration** Collaboration, K. Abe *et al.*, "The T2K Experiment," *Nucl.Instrum.Meth.* **A659** (2011) 106–135, arXiv:1106.1238 [physics.ins-det].

[155] **NOvA Collaboration** Collaboration, D. Ayres *et al.*, "NOvA: Proposal to build a 30 kiloton off-axis detector to study nu(mu) –¿ nu(e) oscillations in the NuMI beamline," arXiv:hep-ex/0503053 [hep-ex].

[156] "The International Design Study for the Neutrino Factory.". URL: https://www.ids-nf.org/wiki/FrontPage.

[157] M. Day and K. S. McFarland, "Differences in Quasi-Elastic Cross-Sections of Muon and Electron Neutrinos," *Phys.Rev.* **D86** (2012) 053003, arXiv:1206.6745 [hep-ph].

[158] A. De Rujula, R. Petronzio, and A. Savoy-Navarro, "Radiative Corrections to High-Energy Neutrino Scattering," *Nucl.Phys.* **B154** (1979) 394.

[159] O. Benhar, A. Fabrocini, S. Fantoni, and I. Sick, "Spectral function of finite nuclei and scattering of GeV electrons," *Nucl.Phys.* **A579** (1994) 493–517.

[160] A. Bodek and J. Ritchie, "Fermi Motion Effects in Deep Inelastic Lepton Scattering from Nuclear Targets," *Phys.Rev.* **D23** (1981) 1070.

[161] M. Martini. Private communication via G. Zeller.

[162] **VLHC Design Study Group** Collaboration, G. Ambrosio *et al.*, "Design study for a staged very large hadron collider,". SLAC-R-591; FERMILAB-TM-2149.

[163] R. Bayes, A. Laing, F. Soler, A. Cervera Villanueva, J. Gomez Cadenas, *et al.*, "The Golden Channel at a Neutrino Factory revisited: improved sensitivities from a Magnetised Iron Neutrino Detector," *Phys.Rev.* **D86** (2012) 093015, arXiv:1208.2735 [hep-ex].

[164] C. Andreopoulos *et al.*, "The GENIE Neutrino Monte Carlo Generator," *Nucl. Instrum. Meth. A* **614** (2010) 87–104, arXiv:0905.2517 [hep-ph].

[165] **Geant4** Collaboration, J. Apostolakis and D. H. Wright, "An overview of the GEANT4 toolkit," *AIP Conf. Proc.* **896** (2007) 1–10.

[166] A. Cervera-Villanueva, J. J. Gomez-Cadenas, and J. A. Hernando, "'RecPack' a reconstruction toolkit," *Nucl. Instrum. Meth.* **A534** (2004) 180–183.

[167] **MINOS** Collaboration, D. G. Michael *et al.*, "The Magnetized steel and scintillator calorimeters of the MINOS experiment," *Nucl. Instrum. Meth.* **A596** (2008) 190–228, arXiv:0805.3170 [physics.ins-det].

[168] K. Kodama, N. Ushida, G. Tzanakos, P. Yager, V. Paolone, *et al.*, "Muon-neutrino to tau-neutrino oscillations: Proposal,".

[169] S. Dixon *et al.*, "NuMI Project (SBL MI-40)," 1994. Project Definition Report No. 6-7-1, April 1994.

[170] S. Henderson, R. Dixon, and W. Pellico, "Fermilab Proton Improvement Plan Design Handbook," 2012. Beams Document 4053-v3.

A Physics Potential of HIRESMNU (the Fine Grain Tracker) in νNuSTORM

We enumerate physics papers that will be engendered with the proposed HIRESMNU, the fine grained tracker for the NuStrom Near Detector. The topics/papers are motivated by the published results by NOMAD, CCFR, NuTeV, MiniBOONE, etc. experiments. Criteria for choosing the topics are as follows:

1. Best Measurement: If the topic deals with a Standard Model measurement then it should be most precise;
2. Most Sensitive Search: If the topic involves a search then it should be the most sensitive search; and
3. New Method: Where 1 and 2 abive are not applicable then the topic should include a novel measurement technique.

In all, we have identified over 80 topics. The list is not complete. For example, it does not include topics involving detector development, R&D measurements, or engineering research that typically are published in journals like NIM, IEEE, etc. The list comprising absolute cross-section measurements, exclusive and semi-exclusive channels, electroweak physics, perturbative and non-perturbative QCD, and searches for new physics illustrates the power of a high resolution, fine-grain-tracker based on the past experiments; and the outstanding physics potential of HIRESMNU. Over the duration of the project, 10 years, the number of theses/paper will be more than twice as many as the number of topics.

Below we present a salient subset of physics topics.

1. Measurement of the absolute neutrino/anti-neutrino flux using neutrino-electron neutral current scattering;
2. Measurement of the difference in the energy-scale of $\overline{\nu}_\mu$- versus ν_e-induced charged-current (CC) events;
3. Exclusive and quasi-exclusive single Pi0 production in neutrino- and anti-neutrino-induced neutral current interactions;
4. Coherent and quasi-exclusive single Pi+ production in neutrino-induced charged current interactions;
5. Coherent and quasi-exclusive single Pi- production in antineutrino-induced charged current interactions;
6. Proton (neutron) yield in inclusive neutrino and anti-neutrino charged current interactions;
7. The ν_e-e^- and $\overline{\nu}_\mu$-e^- interactions and search for lepton number violating process;
8. Measurement of neutrino and antineutrino quasi-elastic (QE) and resonance charged current interactions;
9. Measurement of prompt radiative photon in muon- and electron-neutrino quasi-elastic interactions;
10. Constraints on the Fermi-motion of the nucleons using the 2-track topology of neutrino quasi-elastic interactions;
11. Measurement of the hadronic content of the weak current in neutrino- and anti-neutrino CC and NC interactions;
12. Neutral Current elastic scattering on proton, nu(bar) + p $\rightarrow$ nu(bar) + p and measurement of the strange quark contribution to the nucleon spin, Delta-S;
13. Tests of sum-rules in QPM/QCD;
14. Measurement of nuclear effects on F_2 and on xF_3 in (anti)neutrino scattering from ratios of Ar, Pb, Fe and C targets;
15. Measurement of strange mesons and hyperon production in (anti-)neutrino charged and neutral current;
16. Measurement of the Λ and $\overline{\Lambda}$ polarisation in (anti-)neutrino neutral current interactions;
17. Measurement of backward going protons and pions in neutrino CC interactions and constraints on nuclear processes;
18. Search for muon-neutrino to electron-neutrino transition and the LSND/MiniBOONE anomaly;
19. Search for muon-antineutrino to electron-antineutrino transition and the LSND/MiniBOONE anomaly; and
20. Search for heavy neutrinos using its electronic, muonic and hadronic decays.